Sand Mining Influence on Flooding along
La Colle River in Port Vila, Vanuatu

（バヌアツ・ポートヴィラにおけるラコレ川の洪水に対する川砂採取の影響）

Iuma Bani

201921246

January 2021

A Master's Thesis Submitted to
The Graduate School of Life and Environmental Sciences,
the University of Tsukuba
in Partial Fulfillment of the Requirements
for the Degree of Master of Environmental Sciences

Abstract

Floods are increasingly becoming threats in areas where humans turn to settle. While change in climate may be the primary cause of flooding, sand mining should also be considered. In recent decades, the global sand demand has increased due to economic growth. Increasing amount of sand and gravel are mined each year to satisfy the growing demand from construction and land reclamation. Studies have shown that over-mining riverbeds, floodplains, and deltas have put unprecedented pressure on rivers – and demand is only projected to rise as urbanization and growth absorb more and more sand. Like other third world countries, economic development is one of the main objectives of the island nation, Vanuatu. While being cautious about climate change effects, the government allowed a controlled sand mining activity on La Colle river. This led to the purpose of this study, where investigations are made to understand the influence of sand mining on flood along La Colle river – where the river channel is modified based on sand mining activity, then simulate flood to see how the changing landscape affects flooding.

The employed methodology in this study includes rainfall-runoff analysis, determination of flood return periods, and stream runoff and stage analysis. The precipitation-runoff processes are simulated using The Hydrological Modeling System (HEC-HMS), – where various mathematical models are used to simulate evapotranspiration, infiltration, excess precipitation transformation, and baseflow. Field measurements and Manning's equation were used to verify the simulated discharge. The U.S. Army Corps of Engineers' River Analysis System (HEC-RAS) is used in the stage and discharge analysis. RAS Mapper, a HEC-RAS extension, is used to modify the river channel based on sand extraction activities. The channel was modified by widening and deepening sand extraction areas to a depth of −1, −2, and −3m from the current stream depth. Simulations were done on the original and modified terrains to see how a 10-, 50-, or a 100-year flooding event would behave over the terrains.

Rainfall-runoff results for the 10-, 50-, and 100-year flood return periods were $150 \text{m}^3/\text{s}$, $184.2 \text{ m}^3/\text{s}$, and $408.8 \text{ m}^3/\text{s}$, respectively. Flood simulation results on both original and modified terrain revealed that sand mining could, as well as could not, affect flooding along La Colle river. Total inundated area has reduced by 18% during the 100-year return period when the channel is modified. Meaning, properly controlled in-stream mining on smaller streams could reduce flooding. The controlled small-scale sand mining practice currently happening at La Colle river will not influence flooding.

Keywords: *sand mining, river, flood, HEC-RAS*

Table of Contents

List of Tables

List of Figures

vii

List of Appendices

List of Acronyms and Abbreviations

1D	One-Dimensional
2D	Two-Dimensional
ADB	Asian Development Bank
AULOS	Advanced Hydraulic Modelling System
AWS	Automatic Weather Station
BECA	Beca Group Limited
LiDAR	Light Detection and Ranging
DEM	Digital Elevation Model
DID	Department of Irrigation and Drainage
DOWR	Department of Water Resources
EIA	Environmental Impact Assessment
ENSO	El Niño–Southern Oscillation
GIS	Geographic Information System
GNS	Geological and Nuclear Sciences
GPS	Global Positioning System
GSI	Geological Survey of India
HBV	Hydrologiska Byråns Vattenbalansavdelning
HEC-RAS	Hydrologic Engineering Center-River Analysis System
HEC-HMS	Hydrologic Engineering Center-Hydrologic Modeling System
MAP	Mean-Areal Precipitation
NSE	Nash Sutchliffe model Efficiency coefficient
NZG	New Zealand Government
RI	Recurrence Interval
SANDRP	South Asia Network on Dams, Rivers and People
SCS	Oklahoma Climatological Survey
TACA	Texas Aggregate and Concrete Association
T.C.	Tropical Cyclone
UNEP	United Nation Environmental Program
UNU	United Nations University
U.S.	United States
USACE	United States Army Corps of Engineers
USDA	United States Department of Agriculture
VANSO	Vanuatu National Statistics Office
VMGD	Vanuatu Meteorology & Geo-Hazards Department

WWF   World Wide Fund for Nature

Acknowledgment

I would like to acknowledge the following people who have helped me in this research; without the help and support given me, I would not have made it through my master's degree!

My supervisor Dr. Michiaki Sugita, you have allowed me to study under your supervision. Thank you for your understanding, advice, and guidance throughout this study. Without your help, I would not make it this far.

Japan International Cooperation Agency (JICA), your Pacific Leaders' Educational Assistance for Development of State (P-LEADS) program, has allowed me to learn from the best. Knowledge gained through this research will help tackle flood and sand mining issues in the Pacific and better strengthen Vanuatu and Japan's relationship. Your assistance is greatly appreciated.

The VMGD team at the Ministry of Climate Change in Vanuatu, especially to my co-workers Mr. Dan Tari, Mr. Levu Antfalo, and Mr. Frankie Peter. Thank you for extracting and sending over the hydrological data every month. A special thanks to the Climate Change Division manager Mr. Allan Rarai and your team for allowing me to have access to the meteorological data used in this research.

My colleague at the DOWR, especially Mr. Morrison, you have supported me with much-needed explanations on La Colle's past hydrological data. You have been tremendous by allowing me to stop by your house whenever I have questions.

My biggest thank you to my family and friends for all the support you have shown me through this research, the culmination of two years of distance learning. My fellow P-LEADS scholars at the University of Tsukuba, Miss Matagi and Mrs. Manaka, sorry for being even grumpier than usual while writing this thesis! You two have been my family away from home. And for my mom Ephenster Bani, thank you for all your support, without which I would not have completed this study.

You all have been amazing, and I can only thank our Heavenly Father for allowing our paths to cross to better our small island nation, Vanuatu.

CHAPTER ONE: INTRODUCTION AND BACKGROUND

1.1 Introduction

Vanuatu is an island nation composed of 83 islands located in the South Pacific. The map of the island nation and its geographic location is shown in Figure 1. It is one of the most disaster-prone countries which frequently experience cyclones, volcanoes, earthquakes, and floods (UNU 2015). Like other pacific island countries, Vanuatu is also regarded as a projected 21st-century climate change indicator, from the active onset of El Niño–Southern Oscillation (ENSO) variations, tropical cyclone frequency and intensity changes, and shoreline erosion due to sea-level rise (Mimura 1999). Mimura (1999) also stated that a common threat to the Pacific islands is inundation and flooding, as most islands have a low-laying setting. The increased population migration rate then exacerbates the problem in the capital cities.

As climate change impact continues to threaten Pacific island nations' livelihood, the government and stakeholders must engage in the development and implementation of mitigating strategies that are achievable technically, financially, and politically (ADB 2010).

On March 13th, 2015, Vanuatu was hit by a category five (5) tropical cyclone (TC) Pam. When assisting on the evacuation of people living in flood-prone areas, especially along the La Colle river, it is evident that the country needs to address flood issues on a national level, from flood forecasting, flood mitigation approaches, and further studies on river-related issues. In January 2019, the government prohibited coastal sand extraction while providing an alternative for construction businesses to extract sand along the river. This is because sand is an essential commodity within the industrial world (Work 2016).

On the other hand, sand mining activities are often considered unsustainable as they could destroy the environment leaving irreversible impacts (Asabonga et al. 2016). While La Colle river is currently the only site where controlled sand extraction operates, it is important to understand its impact on the environment and its influence on flooding. This research attempts to discover and understand the relationships between sand mining and flooding along the La Colle river.

1.2 Research gap

Numerous studies have demonstrated that sand mining does have several impacts on rivers. Loss of vegetation, land sliding, and erosion were several sand mining impacts on rivers (Mngeni et al. 2016). In Vietnam, mining upstream of the Lancang river resulted in a very rapid abrasion and removal of crucial sediments for agriculture downstream (Mai et al. 2019). Studies also confirmed mining affects stream flow velocity, which may cause frequent modification

from braided to single-thread channel morphologies, leading to unforeseen flood situations (Yehalegaonkar et al. 2014).

According to Stebbins (2006), sand mining impacts may be classified into three categories. First, the physical effects; mining from streambed causes alteration of channel slope and the channel morphology. Second, the water quality impacts; mainly due to dredging activities, reducing water quality for downstream users, and increasing treatment costs. Third, the ecological impacts; the loss of habitats and species disturbance. More detailed potential effects of sand extraction were discussed in the literature by (Rinaldi et al. 2005), which includes:

a) Riverbed degradation and its effects on channel bank and its stability.
b) Relationship between sediment load and water clarity
c) Channel morphology changes and its ecological effects on river habitat
d) Channel modification and riverbank erosion
e) Heavy equipment impacts on extraction sites
f) Changes in groundwater level due to sand mining
g) Sand mining impact on coastal procedures

Previous studies noted that the science behind the link between sand mining and flooding could be a little murky. Rehak (2019) argued that the San Jacinto River in Texas was flooded during Hurricane Harvey in 2017 because sand mining occurred on the river for the past decade. Instead, TACA (2018) claimed that sand mines, far from being responsible, held back some floodwaters, reducing flooding. In such a case, we could assume sand mining might not seem controversial in some respects. They could also be a benefit, while on the other hand, they are an issue. As such, more research into the science behind sand mining and river flooding is required.

Previous studies on sand mining indicated that most studies were done in areas outside the Pacific region and in larger rivers. While small scale sand mining in smaller rivers is happening in the Pacific, there is also a need to guard the environment and reduce potential flood issues. Hence, the need for this study within the region.

1.3 Research goal
To investigate the influence of sand mining on flooding along La Colle river.

1.4 Specific objective
• To complete hydrological field investigations
• To analyze obtained hydrological and meteorological data

- To simulate flood on original and modified terrain
- To make recommendations accordingly

1.5 Research area

Vanuatu is made up of a mixture of islands having either a volcanic or a coral origin. At least 35% of the country is above 300 meters, with approximately 55% of the islands have slopes greater than 20°. Dense tropical forests cover most islands in Vanuatu. (SPREP 2001). Agricultural activities are generally located around the coastal areas, while typical gardens are located on the edge of the cultivated areas, progressing into the non-cultivated areas.

Although Port Vila, Luganville, and Lenakel have ample population size, most Ni-Vans live in rural areas. Port Vila has grown into the country's largest city, which accounts for 19% of its population. (VANSO 2020). The country has a growth rate of 2.4% per year, which also increases the migration rate to urban environments. With increasing urban movement, settlements are being developed near or within potential flooding areas. La Colle river is approximately 6 km from Port Vila, making it an ideal spot along its banks for agricultural activities. The river also acts as a divider between the urban and semi-urban areas. Figure 2 shows the study area map and its location outside Port Vila.
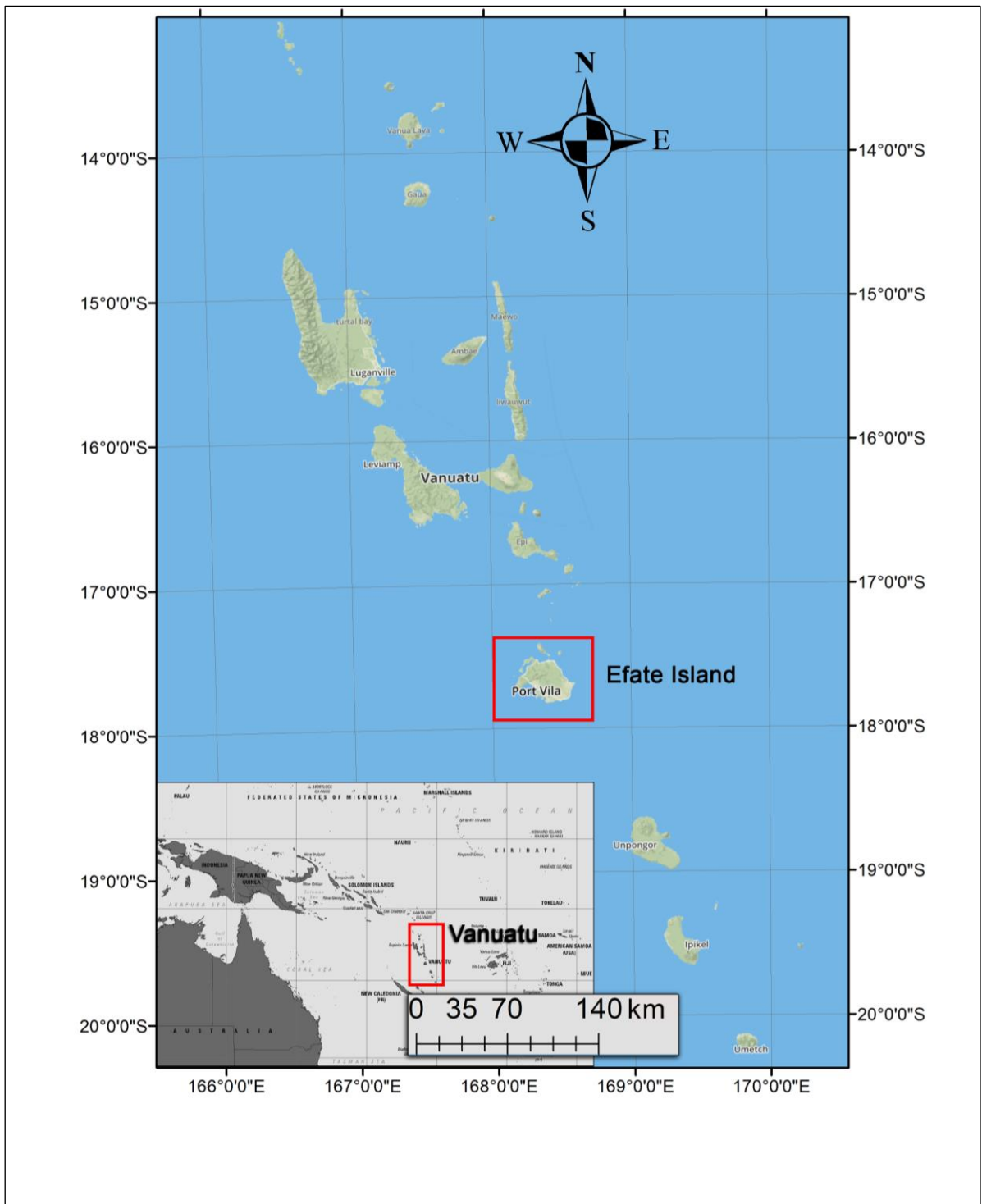
Figure 1. Geographic location and the map of Vanuatu
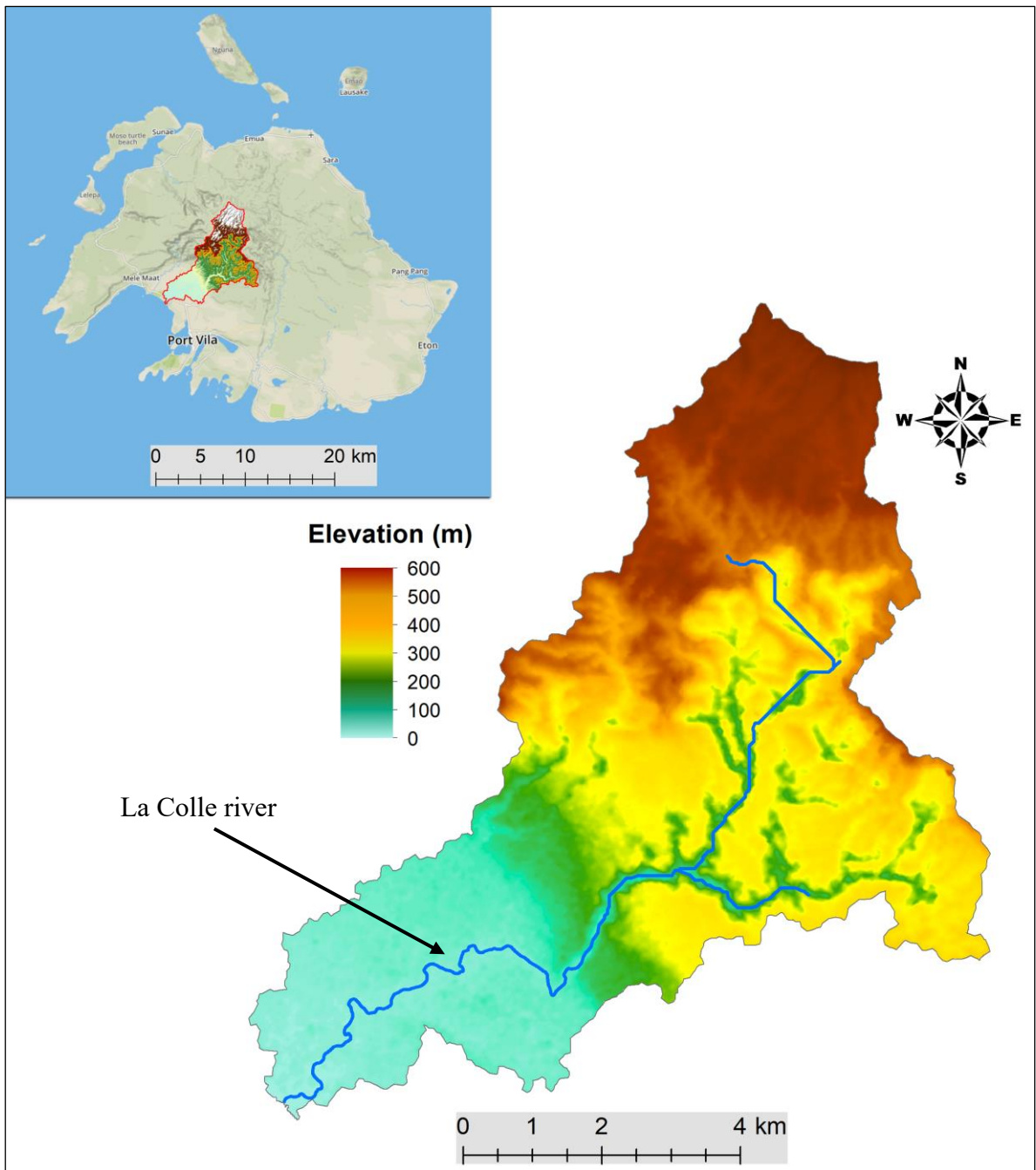
Figure 2. Map of study area

La Colle river is located within the Mele catchment, with approximately 150 km^2 of land (Beca et al. 2015). The study area covers an area of 50 km^2 with an elevation of 1 – 602m.

Based on how each of the islands formed, the study area contains a mixture of silt and sand. The country's climate varies from a wet tropic in the north to a much dryer subtropical in the southern islands. Average temperature ranges from 21°C to 27°C, with an average humidity of about 78 %. A decline in average annual rainfall from the north to the south shows that 4000 mm is recorded in the north while a little less than 1500 mm in the south (Brock 1998).

1.6 Summary

The chapter introduced the research topic and discussed the research gaps, goals, and objectives. Discussions in the next chapter are based on reviewing past research articles relating to sand mining and flooding.

CHAPTER TWO: LITERATURE REVIEW

2.1 Introduction

This section gives a general description of the term mining and the methods used to evaluate their impact on runoff and flooding. Basics of stream dynamics will be first discussed before taking a closer look into current sand mining practices and analysis.

The process of extracting sand and other deposits along the river channel or within a river's floodplain is called sand mining (EIA 2012). The extraction site can be both along the coast or further inland in areas like dunes, abandoned channels, and gullies (Dhakwa et al. 2005). Since sand can also be presented in various shapes and sizes, Saviour and Stalin (2012) defined sand mining as the process of sand removal to an extend where it becomes an environmental issue. Equally, UNEP (1991) described it as either a temporary or a permanent lowering of land with a productive capacity.

There are hydraulic relationships within the extraction site that are needed to be considered when extracting sand. These relationships include factors like the extraction depth, water table, stream shape, and channel size. Therefore, a better understanding of such relationships can lead to a sustainable (minimal environmental impact) in-stream or near-stream sand extraction activity.

Other sand mining practices apart from in-stream or near-stream includes dry pit and wet pit mining. Figure 3 shows where these extraction practices normally happened along the river channel. Dry pit mining involves excavating dry ephemeral stream beds, while wet pit mining involves mining a perennial channel below the water level (DID 2009). Another sand extraction practice is called scraping. This is when sand is removed from the top portion of the bar deposits: usually done with a sustainable mining intention. Sand mining the river channel largely depends on the geomorphology of the area. As seen in Figure 3, dry pits are located above the water level, while shallow wet pits are located below the water table (EIA 2012).
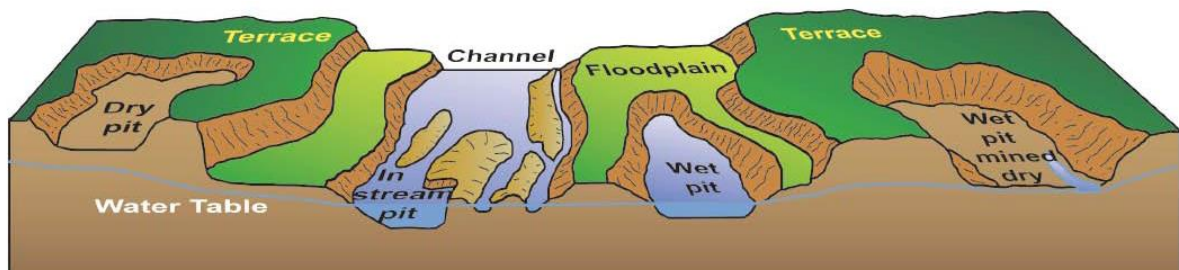
Figure 3. Possible aggregate extraction locations

EIA (2012) further emphasized the two sand extraction methods, the mechanical and the hydraulic dredging method. The mechanical method involves using construction types of machinery such as excavators, backhoes, and bulldozers. This approach is widely used in shallow rivers. A mechanical method example is shown in Figure 4, where a backhoe can be seen loading sand onto a heavy-duty truck in India (SANDRP 2019).

The hydraulic Dredging method involves specially built sand-dredging equipment. This method extracts sand by either dragging or suction. Usually, a suction pump is sited on a pontoon. This method is normally used for larger-scale operations and on large rivers.

Figure 4. Mechanical method used in sand extraction. SANDRP (2019).

2.2 Sand mining impacts on river runoff and inundation

Rivers are complex systems with their primary function to transport water and sediment. The work demanded of a river is determined by the climate, geology, topography, and vegetation characteristics of the basin (Langer 2003). Cross-sectional shapes and the meander and braiding patterns of a river continuously adapt to the flow and sedimentological conditions that reflect the history of flow events (EIA 2012).

Each river is unique, and over time, it develops a particular combination of certain variables. These variables include the channel's width, depth, slope, roughness, particle size, and stream velocity. When combined, the variables are called the hydraulic geometry, through which the stream is enabled to perform in the best possible manner. When a river's hydraulic geometry has been established, it will be maintained provided that the variable(s) variations are within the current hydraulic geometry limits.

Small discharge and load changes in a river are easily accommodated with minor changes on the channel (Langer 2003). Stream channels normally undergo changes during a relatively larger flow than normal. After such an event, the channel's hydraulic geometry will be readjusted, and a new equilibrium is developed. Since the variables are codependent, changing one variable will result in a change in the other variables also.

Active streaming channels contain dynamic properties that respond quickly to outside stimuli, including sand extraction. (Kori and Mathada 2012). As such, they can accommodate changes made on the channel without creating unfavorable environmental impacts if sand mining operates within the hydraulic conditions set by the stream. (Kondolf 1994). Sand mining should be conducted only after careful consideration, as failure to do so could result in a series of environmental problems, either within the extraction area or in other areas along the channel (EIA 2012).

The negative impacts of sand mining on runoff and flooding, according to GSI (2016), includes:

i. Lowering the groundwater table: Mining could lower the riverbed, which in turn decreases the water level, resulting in the lowering of the groundwater table. This could trigger a scarcity of water for vegetation, livestock, and human settlements within the vicinity.

ii. Groundwater depletion: excessive groundwater pumping during sand mining generally decreases the groundwater level. This could cause severe scarcity of water and could affect water availability. In severe cases, it may cause an increase in ground fissures and could also lead to land subsidence in the surrounding areas.

iii. Groundwater pollution: In cases where the river is recharging the groundwater, mining could reduce the sediment's thickness. Thus, reducing water quality during

infiltration since the sediments acts as a natural filter when groundwater is recharged. Pollutants from mining activities, such as washing of mining materials, removal of wastes, diesel, and vehicular oil lubricants, could also contaminate groundwater.

On the other hand, according to Osanloo and Mobtaka (2014), sand mining does positively impact stream runoff and flooding. It is because sand mining sites could control surface water and runoff during a heavy rainfall event. Moreover, the removal of sand in or beside the river channel, if done correctly, will provide a larger storage capacity. In doing so, it will allow the channel to hold a larger runoff amount. Furthermore, in areas where lakes have been built to store sediments, the lakes can also act as a network of dams controlling excess runoff and flooding during an extreme event. Mining is seen here as an option to minimize material losses. There are cases where organized and controlled mining prevents nearby towns and settlements from being frequently flooded (Borsanyi 2014).

2.3 River runoff and inundation estimates

Many studies have been done on river runoff and inundation estimates over the years. Most of which mainly focused on original basin terrain. Since changes in channel morphology include aggradation and degradation, such changes are site-specific and require specialized investigations.

Models are used in estimating runoff and inundation, and they are used in different study cases based on their performance with regards to the study area's characteristics. Methods used for estimating inundation also vary extensively. However, all are founded on fluid hydraulics. Specifically, they differ in how they represent reality; 1-D models consider streamflow along a particular line, while 3-D models consider both flow depth and flow width (NZG 2010).

With 1-D models, the river channel is represented by many cross-sections closely spaced together to accurately determine the topography features. Other properties of these cross-sections include a constant average velocity with a flat-water surface. When creating the channel's geometric data, the designer determines the flow paths; otherwise, flow circulation patterns cannot be resolved. Beretta et al. (2018) also acknowledged that in areas with a lower terrain slope, 1-D models might produce inaccurate results. Therefore, 2-D models are recommended since they can capture preferential flow directions produced because of newly built structures along the channel. Finally, 1-D models can interpolate the extent of the simulated flood to create a flood map. AULOS, MIKE-11, and HEC-RAS are examples of 1-D models. As suggested by Andrei et al. (2017), one must bear in mind that some of these 1-D

models may not have the ability to simulate supercritical flow, which could result in inaccurate model predictions.

   2-D models apply the same principle as a 3-D model when describing a river and its flood plains. Such models accommodate varying stream velocity and depth in all horizontal directions and reproduce plan-form flow circulation patterns. Furthermore, at any point in time, stream velocity across the water surface is the same as that at the bed (depth-averaged flow). The ground topography and roughness determine flow paths. While the model results neatly show water level depth and velocity at each DEM node, it may take a while to compute complicated situations depending on the computer's specifications. Several models use 1-D equations in their computations when dealing with stream channel and 2-D equations involving floodplains. Hydro-2de, RiCOM, and MIKE21 are some examples of 2-D models (NZG 2010).

   HEC-HMS and HEC-RAS are two models used in this research in determining the rainfall-runoff and the discharge-stage relationship. Generally, the steps involved in rainfall-runoffs and inundation estimates are shown in Figure 5.

Figure 5. Steps involved in rainfall-runoff and inundation.

When estimating rainfall, the common techniques used are the Thiessen Polygon (T.P.) Method, Kriging Method (K.M.), Reciprocal Distance Squared (R.D.S.) Method, and the Multiqua-dric Equations (M.E.) Method. However, when dealing with stream flooding, hydrologists use return periods. Simply stated, a return period estimates the amount of time between rainfall of a given magnitude. (OCS 2005). As demonstrated by Eidukat (1997), to estimate the likelihood that any discharge will equal or exceed a specified limit in a year, peak discharge amounts are ranked from the largest to the smallest: $m = 1$ is the largest till $m = n$, where n is the number of years on which the data was taken. Using the Weibull equation, a Recurrence Interval (RI) is determined for each data point:

$$RI = (n + 1)/m \hspace{4cm} \text{Eqn. 1}$$

RI can be defined as the projected average time between two larger storm events. (Lundgren 1986).

   Once the return periods are determined, each return period's total rainfall amount is converted into runoff. Several methods used in achieving runoff based on rainfall were recorded by Nash et al. (1958). The initial methods include:

- The Rational Method
- The Tangent Method
- The Time-Area Methods
- The Unit-Hydrograph Theory
- The Modern form of the Unit-Hydrograph Theory

In the 18th century, more scientific approaches were being developed, including Bernard's approach, McCarthy's approach, Synder's approach, Taylor, and Schwarz's approach. Supported by advances in the physical understanding of hydrological processes, hydrology has been approached with a more theoretical basis along with the advent of computers and Geographic Information Systems. Modern hydrological models are capable of integrating refined versions of the approaches mentioned above. For example, to determine the gage weighting factors for Mean-Areal Precipitation (MAP) depth, HEC-HMS uses the TP method. This method assumes that at any point within a watershed, that point's precipitation depth is equal to the nearest gage's precipitation depth to that point (Feldman 2000).

Figure 6 shows how the TP method is being applied in a watershed with several gages. It shows that points closest to each gage are found by drawing a line connecting the gages, then another line perpendicular to the connecting line is drawn – through the center of the connecting line. The lines then form a polygon around the gage, and all points within that polygon share the same precipitation depth as the gage. Each polygon area near the gage is then assigned the weight, which is the fraction of the polygon's total area.
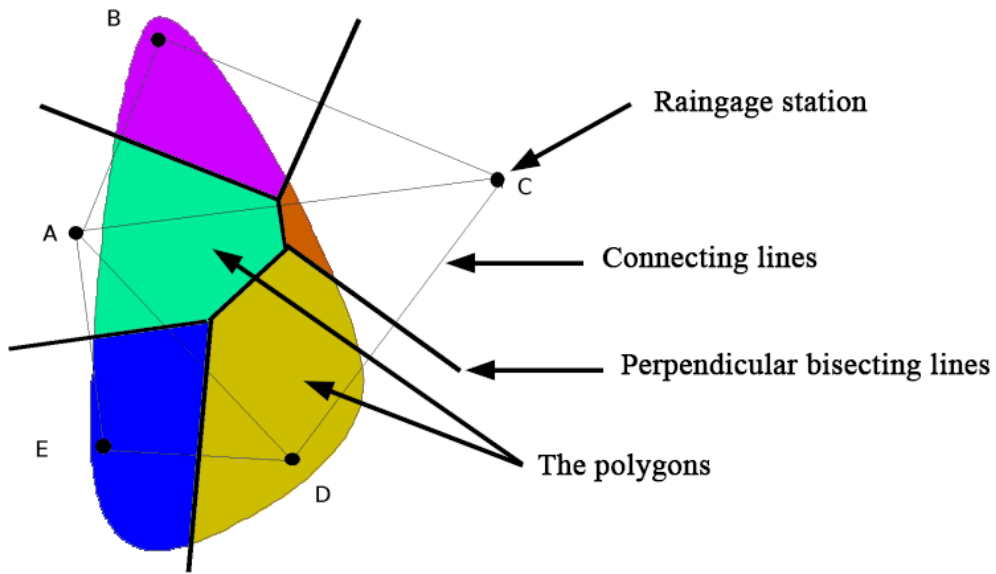
Figure 6. Assigning areal significance to point rainfall values using Thiessen polygon method. USACE (2000).

Within a watershed, several models are used to simulate potential runoff from excess precipitation. Discussed below are two transformation methods.

1. Empirical Models: They are also referred to as data-driven models, where non-linear statistical relationships are used between inputs and outputs. They rely heavily on input accuracy as they are observation-based (Kokkenen et al. 2001). Eqn. 2 shows the empirical models' governing equation that depends on the inputs:

$$Q = f(X, Y)$$

<div align="right">Eqn. 2</div>

where the runoff output is Q, and the input datasets of rainfall and historic runoff are X and Y, respectively.

According to (Beven 2012), the internal processes that govern how runoff outcomes are determined are somewhat hard to explain. It is because the functions used in the rainfall-runoff transformation process are either an unknown procedure or without any description of a physical process.

For the Curve Number method, there are two phenomena the method is based on, before and after runoff begins. Before runoff begins, the initial accumulation of rainfall is called initial abstraction. This includes interception, depression storage, and infiltration. When rainfall is lost due to the infiltration process after runoff has started, it is called actual retention. The relationship between rainfall amount and the actual retention is directly probational to each other. As rainfall increases, so does the actual retention until it reaches some maximum value: the potential maximum retention. The mathematical relationship between the two phenomena assumes that the actual retention to potential maximum retention ratio equals the actual runoff to potential maximum runoff ratio. This mathematical relationship is expressed as:

$$\frac{F}{S} = \frac{Q}{P - I_a}$$

<div align="right">Eqn. 3</div>

where,

F = actual retention (mm)

S = potential maximum retention (mm)

Q = accumulated runoff depth (mm)

P = accumulated rainfall depth (mm)

I_a = initial abstraction (mm)

Once runoff has begun, excess rainfall will now be either runoff or actual retention. Mathematically, it is express in Eqn. 4.

$$F = P - I_a - Q \qquad \text{Eqn. 4}$$

When combining Eqn. 3 and Eqn. 4, we get

$$Q = \frac{(P-I_a)^2}{P-I_a+S} \qquad \text{Eqn. 5}$$

However, Eqn. 5 still has two variables that are needed to be estimated, I_a and S. So, a regression analysis was developed from documented rainfall and runoff data on small catchment areas. The results displayed a vast amount of scattering, and the relationship was found:

$$I_a = 0.2S \qquad \text{Eqn. 6}$$

Combining Eqn. 5 and Eqn. 6, we get

$$Q = \frac{(P-0.2S)^2}{P+0.8S} \text{ for P} > \textit{0.2}\text{S} \qquad \text{Eqn. 7.}$$

Eqn. 7 is the rainfall-runoff relationship used in the Curve Number Method. Given the potential maximum retention S, the runoff depth can be estimated from the rainfall depth.

The potential maximum retention S is then converted to the Curve Number CN so that interpolating, averaging, and weighting operations are more linear. The relationship is expressed in Eqn. 8.

$$CN = \frac{25400}{254+S} \qquad \text{Eqn. 8}$$

Figure 7 illustrates the graphical representation of Eqn. 8, indicating runoff depth Q values as a function of rainfall depth P for selected Curve Number values.
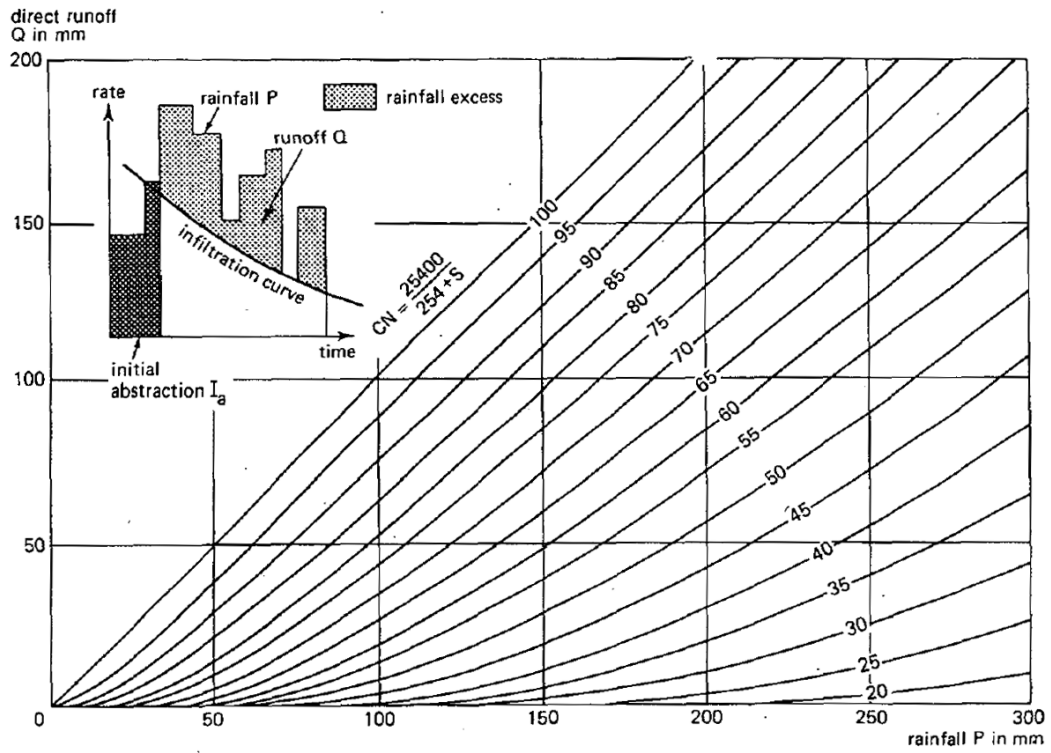
Figure 7. A visualization of the empirical Curve Number method. (http://edepot.wur.nl/183157)

Ungauged drainage basins are better modeled by an empirical method because there may be a lack of specific information required, as fewer parameters are needed – making these models easy to use. However, they can be very reliable in certain cases, including recreating past rainfall and runoff in short periods (Vaze et al. 2012). SWAT2, HEC-HMS, and the regression equations are examples of empirical models that use the CN method.

2. Conceptual Models: These models are built based on observed or assumed empirical relationships among different hydrological variables. Unlike empirical models, which only consider the statistical relationship between precipitation and runoff, the water balance equation is represented by the conceptual models with the rainfall-runoff conversion, evapotranspiration, and groundwater. Mathematical equations that distribute the precipitation input data estimate each component in the water balance equation (Sitterson et al. 2017). Governing equations for conceptual models are versions of the water balance equation which accounts for surface water and storage fluctuations: see Eqn. 9:

$$\frac{dS}{dt} = P - ET - Q_s \pm GW \qquad \text{Eqn. 9}$$

where *dS/dt* is the change in reservoir storage, *P* is precipitation, *ET* is evapotranspiration, Q_s is surface runoff, and *GW* is groundwater.

Water movements within the atmosphere, hydrological components, and storage reservoirs simulated by conceptual models are based on a balance equation. Beven (2012) states that these models rely on the complexity in which complex balance equations are used to describe hydrological components. As a result, more parameters and meteorological data are needed for input. On the other hand, they are much easier to use and calibrate. A few examples of conceptual models are TOPMODEL, HBV, NWSRFS, and HSPF.

When modeling channel flow, several models are considered. Generally, these models determine a downstream hydrograph, based on an upstream hydrograph. The outcome is achieved by the models solving the continuity and momentum equations. HEC-HMS uses several models:

- Lag
- Muskingum
- Modified Puls, also known as storage routing
- Kinematic-wave

- Muskingum-Cunge

Basic equation for open channels includes the momentum equation and the continuity equation. Combined, the equations become the St. Venant equations or dynamic wave equations (Feldman 2000). As expressed in Eqn. 10 and Eqn. 11, the momentum equation considers the sum of gravitational, pressure, and friction forces to the product of fluid mass acceleration, while the continuity equation accounts for the water volume in an open channel's reach.

The momentum equation in 1-D is as follows:

$$S_f = S_0 - \frac{\partial y}{\partial x} - \frac{V}{g}\frac{\partial V}{\partial x} - \frac{1}{g}\frac{\partial V}{\partial t}$$

Eqn. 10

where

S_f = energy gradient

S_0 = bottom slope

V = velocity

y = hydraulic depth

x = distance along the flow path

t = time

g = acceleration due to gravity

$\partial y / \partial x$ = pressure gradient

$(V/g)(\partial V/\partial x)$ = convective acceleration

$(1/g)(\partial V/\partial t)$ = local acceleration

The continuity equation in 1-D is as follows:

$$A\frac{\partial V}{\partial x} + VB\frac{\partial y}{\partial x} + B\frac{\partial y}{\partial t} = q$$

Eqn. 11

where

B = water surface width

q = lateral inflow per unit length of the channel

Each term in Eqn. 11 describes the inflow to, the outflow from, or a storage along the channel, a lake, or a reservoir. The terms are described by Henderson (1996) as follows:

$A(\partial V/\partial x)$ = prism storage

$$VB(\partial y/\partial x) = \text{wedge storage}$$
$$B(\partial y/\partial t) = \text{rate of rise}$$

Essentially, the derivation of the dynamic wave equation is based on the assumption that:

- The streamflow velocity is constant in the channel, and the water surface is horizontal.
- All flow varies moderately, with hydrostatic pressure being dominant at all points in the flow.
- There is no lateral or secondary circulation.
- Channels have set boundaries where bank erosions or sediment deposition are ignored.

Discussed above are a few of the basic principles currently used by models involving converting rainfall to runoff.

The theoretical basis for 2-D hydrodynamic calculations will be discussed in this section. Discussions are limited to unsteady flow routing. There is an assumption that when studying flow over complex floodplains, flow is 1-D and that it may no longer be valid in 2-D. It is because 2-D unsteady flow varies in time and along two spatial dimensions. The 2-D form of the continuity equation claims that the net mass flux into the control volume equals the storage change in the control volume. However, the difference is that the mass fluxes are now calculated in 2 dimensions. Eqn. 12 expresses the 2-D continuity equation:

$$\frac{\partial H}{\partial t} + \frac{\partial (hu)}{\partial x} + \frac{\partial (hv)}{\partial y} + q = 0 \qquad \text{Eqn. 12}$$

where

H = water surface elevation

h = water depth

u and v = depth average velocities in the x- and y-direction

q = the source term, representing inflow from external sources such as precipitation (Chaudhry 2008).

Similar to the 1-D momentum balance principle while considering forcing from gravity, momentum exchange, friction, and the Coriolis effect, the 2-D momentum balance equations can be written as follows:

Momentum balance in the x-direction

$$\frac{\partial u}{\partial t} + u\frac{\partial u}{\partial x} + v\frac{\partial u}{\partial y} = -g\frac{\partial H}{\partial x} + vt\left(\frac{\partial^2 u}{\partial x^2} + \frac{\partial^2 u}{\partial y^2}\right) - c_f u + fv \qquad \text{Eqn. 13}$$

The momentum balance in the *y*-direction

$$\frac{\partial v}{\partial t} + u\frac{\partial v}{\partial x} + v\frac{\partial v}{\partial y} = -g\frac{\partial H}{\partial y} + vt\left(\frac{\partial^2 v}{\partial x^2} + \frac{\partial^2 v}{\partial y^2}\right) - c_f u + fv \qquad \text{Eqn. 14}$$

where

H = water surface elevation

v_t = momentum exchange coefficient

c_f = friction coefficient

f = the Coriolis parameter

v and u = depth-averaged velocities in the x and y directions respectively (Brunner 2016).

The local acceleration is represented by the first term in the momentum equation $\left(\frac{\partial u}{\partial t}\right.$ in Eqn. 13, corresponding term in Eqn. 14$\left.\right)$, and the convective acceleration is the second term $\left(+u\frac{\partial u}{\partial x} + v\frac{\partial u}{\partial y}\right.$ in Eqn. 13, corresponding term in Eqn. 14$\left.\right)$. Forcing from gravity, momentum exchange coefficient, bed friction, and Coriolis force are the terms that followed. The Manning's formula was used to express the friction coefficient c_f in the x-direction:

$$c_f = \frac{n^2 g |u|}{R^{4/3}} \qquad \text{Eqn. 15}$$

where

n = Manning's roughness coefficient

g = gravitational constant

u = velocity in the *x*-direction

R = hydraulic radius

(Betsholtz and Nordlof 2017).

With regards to the purpose and methodology of this study, a literature review has been done to see how well these equations perform within the HEC-RAS model. Two case studies on the HEC-RAS model with regards to inundation are discussed below.

A case study by Eko et al. (2014) on Pesanggrahan floodplain, Jakarta, compared estimated inundated areas with observed results to assess the modeled results' validity. The

study concluded that the model performance was close to the observed results, especially in areas with fewer structures such as housing and fences. However, technical adjustments are needed in areas where recent structures are being erected. In doing so, the model results could be improved.

Using remote sensing, GIS, and HEC-RAS techniques to validate flood extend on Baseu river, Romania, Enea et al. (2018) concluded that their validation processes were successfully carried out for a series of stages on a case study of Baseu river. Based on recorded hydrological data, floodwater levels generated by HEC-RAS were validated by water levels recorded at the Stefanesti hydrometrical station, with a 9.2% error.

2.4 Summary

This chapter discusses sand mining's different approaches and the common area sand is normally extracted from along the river. Methods used in determining runoff and inundation estimates were also briefly discussed. The next chapter covers the methodology used in this study.

CHAPTER THREE: RESEARCH METHODOLOGY

3.1 Introduction

This chapter discusses the methodology adopted for this study. It covers the study design flow, data collection process, the models used, terrain modification process, and the flood simulation process. Since this study is the first of its kind within the country, data collection was a very big challenge, especially hydrological data. For example, consistent hydrological data, with a time interval of 30 minutes, were collected from two separate sensors installed on the upstream and the downstream of La Colle river in August 2019. Before that, there were no data with a consistent time interval. There were also no previous flood maps that could be used to verify the simulation, making it difficult to estimate the inundated areas correctly.

3.2 Research Design

The study employed a methodology involving three different platforms: Arc-GIS, HEC-HMS, and HEC-RAS. Arc-GIS was used to delineate the study area watershed and prepare geometric data used in HEC-RAS. Upon completion of the simulations, the data are then imported back into Arc-GIS for map development. HEC-HMS is the hydrological model that uses rainfall to determine discharge, while HEC-RAS uses the discharge to determine stream stage (inundated area). HEC-RAS was also used to modify the terrain.

The first phase of the research design workflow involves observational data, meteorological data, and hydrological data. After data collection, HEC-HMS is used to determine the rainfall and runoff relationships (discharge) relationships. The outcome is determined by calibration of the model with respect to observational data. Discharge is then imported into HEC-RAS, where the stream stage is determined. Once stream stage is verified with observational data, stream channel is then modified to gather for sand mining activity. Finally, using the modified terrain, flood simulations are performed, and flooded areas are analyzed. Figure 8 shows the design and workflow process used in this study.
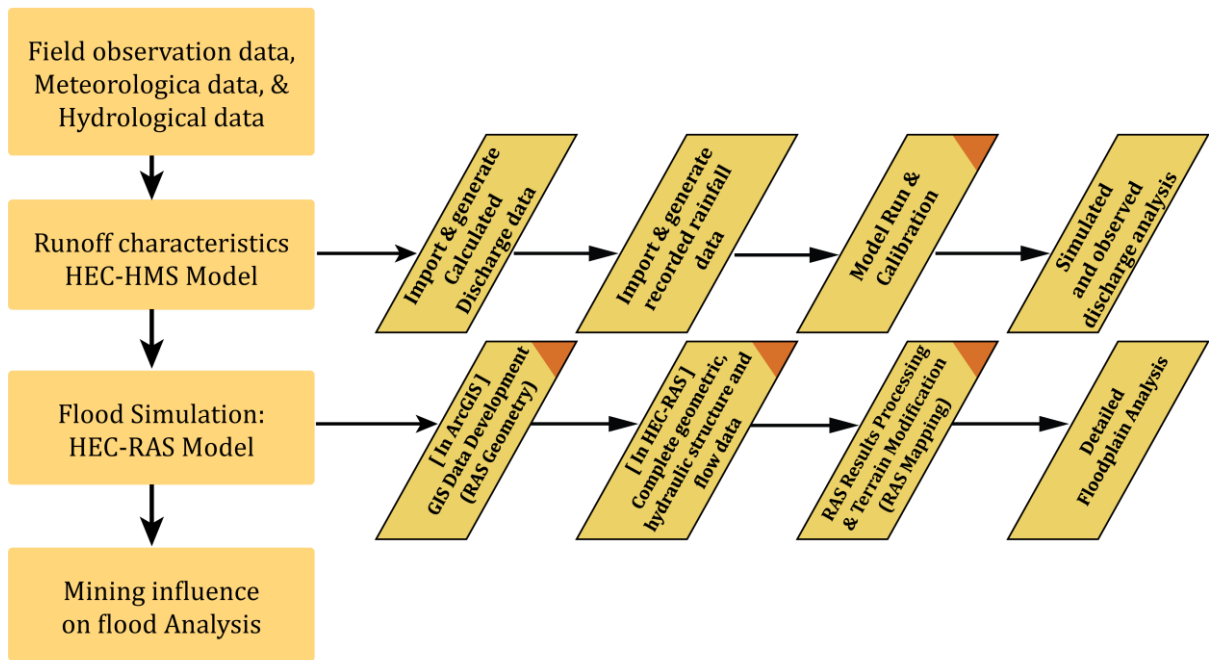
Figure 8. Research design workflow.

3.3 Research Dataset

Table 1 shows the list of data used in this study. Due to time constrain and lack of data, geological and groundwater data were not effectively used in this study.

Hydrological data consist of data extracted from installed water level data logger (sensors) in August 2019. Figure 13 shows the location where the sensors are installed. The water level sensors record changes in water level due to pressure change and later converted to water level depth. The sensors are set to record data every 30 minutes. Data is extracted monthly by VMGD staff members and submit via email to the researcher in Japan.

Figure 13 also shows the location where the Meteorological data was obtained. The data was extracted from an AWS beside the Bauerfield International Airport, with a 10 minute time interval. Unfortunately, this is the only reliable weather station within the study area.

Field observation and investigation data include streamflow cross-sectional area measurements, stream velocity measurements, flood extent investigation, and stream depth measurement after a sand extraction event.

All data types used in this research were based on the local standard time, Universal Time Coordinated (UTC) +11 hours.

3.3.1 Field observation and investigation

In order to verify the accuracy of the provided LiDAR DEM, three sites were chosen to measure the channel cross-sections. These sites were measured on August 15th, 2019. Figure 9 shows the location where the cross-sections are measured. Extracted cross-section data from the LiDAR DEM were then compared with the recorded measurements.

Riverbed cross-sections were measured to modify the river channel. Measurements were done on March 8th, 2020, on 21 different sites along the river reach of about 7 km. Figure 10 shows the cross-section measurement process at four different sites, while Figure 11 shows all the measurement sites along the river reach. The recorded measurements were later used to develop the streamflow cross-sections as the provided LiDAR DEM did not capture the riverbed cross-sections.

Streamflow measurements were done in 4 different sites along the river. As shown in Table 2, the first set of measurements were done in August 2019 during the dry season and the second in March 2020; the wet season. A total of 22 measurements were performed, and the results were used to determine stream discharge amount and the Manning's roughness value. Figure 12 shows the location where the measurements are done, while inserted images of the measurements were done on March 4th, 2020.

To verify inundated areas, the team interviewed local community members about flood extent during TC Pam, a cyclone that hit Vanuatu on March 13th, 2015. The interview

was simple, as the only question asked was to recall and estimate flood extend during TC Pam accurately. Coordinates of the estimated flood extent were recorded using a GPS device. Obtained coordinates were then converted from decimal degree (DD) to degrees, minutes, and seconds (DMS) and are listed in Table 3. Figure 14 shows the obtained coordinates being plotted over the DEM showing flood extent.

3.3.2 Hydrological dataset
The primary hydrological dataset used in this study was obtained from the installed hobo water-level data logger. As seen in Figure 13, two data loggers were installed along the river, one on the upstream and the other on the downstream. The upstream installation was done by Dan Tari, Julius Mala, and the researcher on August 22nd, 2019, from 12:53 to 6:14 pm. The sensor was installed inside a specifically build metal pipe bolted to a cement slab constructed by the DOWR in the 1970s.

The riverbank was dug for the downstream station, allowing the PVC pipes containing the sensors to be buried inside. Two pipes were connected in a letter L shape allowing for the other end of the pipe to be in the river while the other is further away from the river and over the riverbank, yet accessible to the river water level. The installation was done on August 18th, 2019.

Before installing the two data loggers, there was no ongoing hydrological data collection on La Colle river since 1985.

Table 1. List of data used in this research.

	Hydrological Data	Source	Location of Collected Data
1	Water level data (Sept. 2019 - Aug. 2020)	Installed Sensors in August 2019	Upstream and downstream of La Colle river
	Meteorological Data		
1	Rainfall data (2016 - 2020)	AWS	Bauerfield International Airport
2	Rainfall data (1925 - 2017)	Manual station	Bauerfield International Airport
	Field Observation Data		
1	Riverbed cross-section data	Field measurements	21 sites along La Colle river
2	Stream flow data	Field measurements	4 sites along La Colle river
3	Flood extent data	Local community members	Along La Colle river (9 points were obtained)
	Water depth after sand extraction	Field measurements	Sand mining site 1
	Digital Elevation Model		
1	1m LiDAR-Based Digital Elevation Model	PMU Office	Ministry of Climate Change
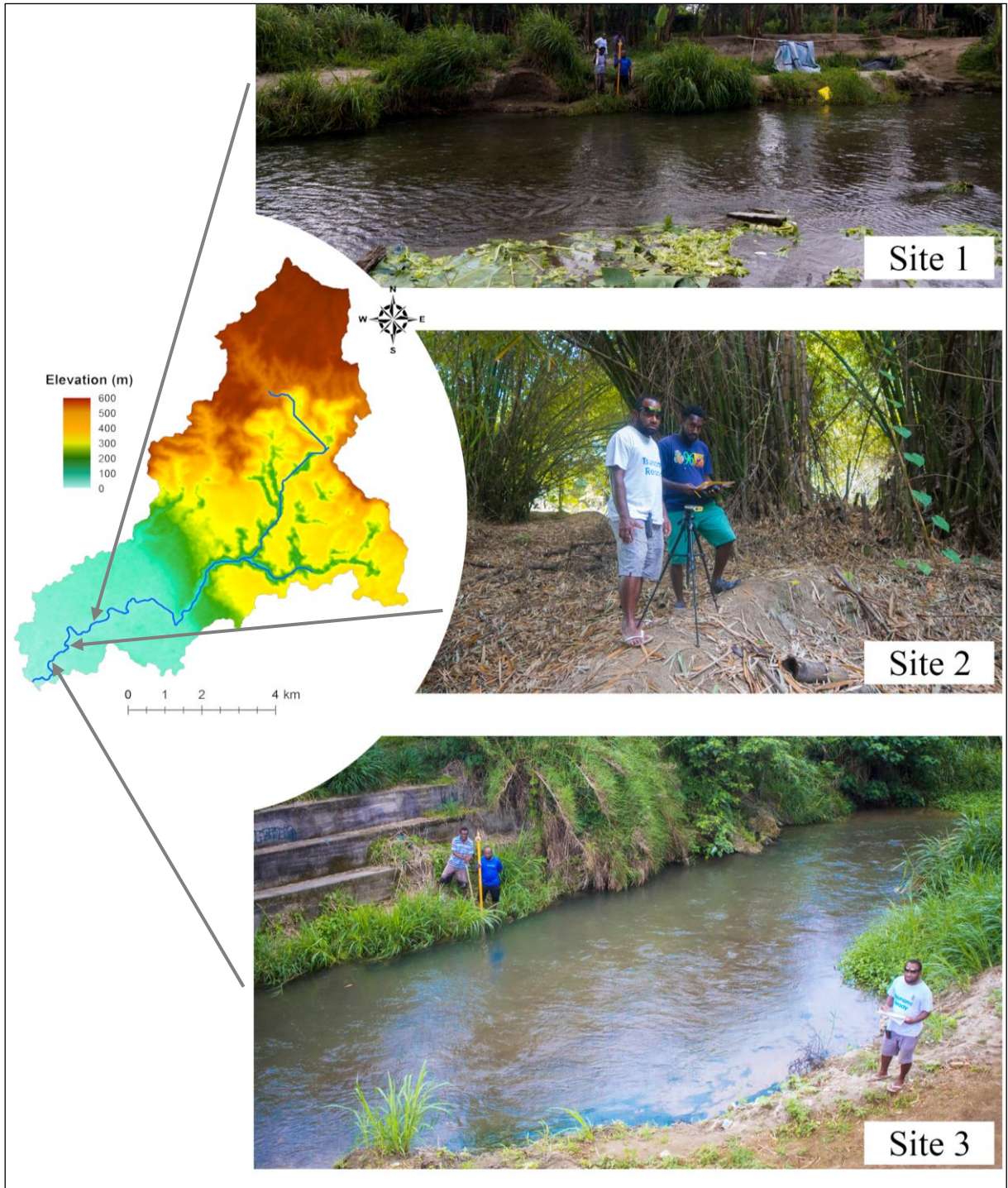
Figure 9. Sites selected for channel cross-section verification.
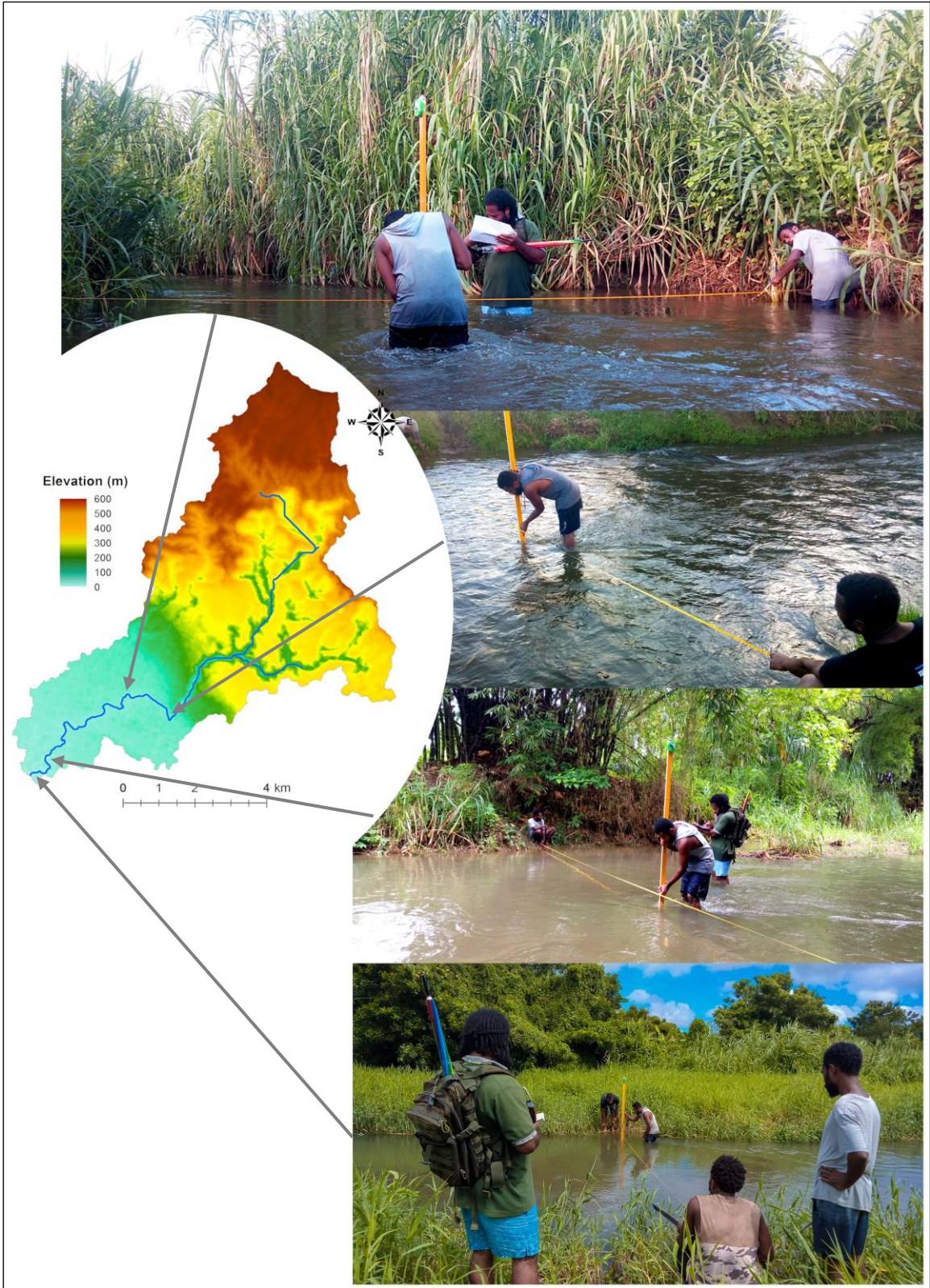
Figure 10. Four of the 21 sites where riverbed cross-sections were measured.
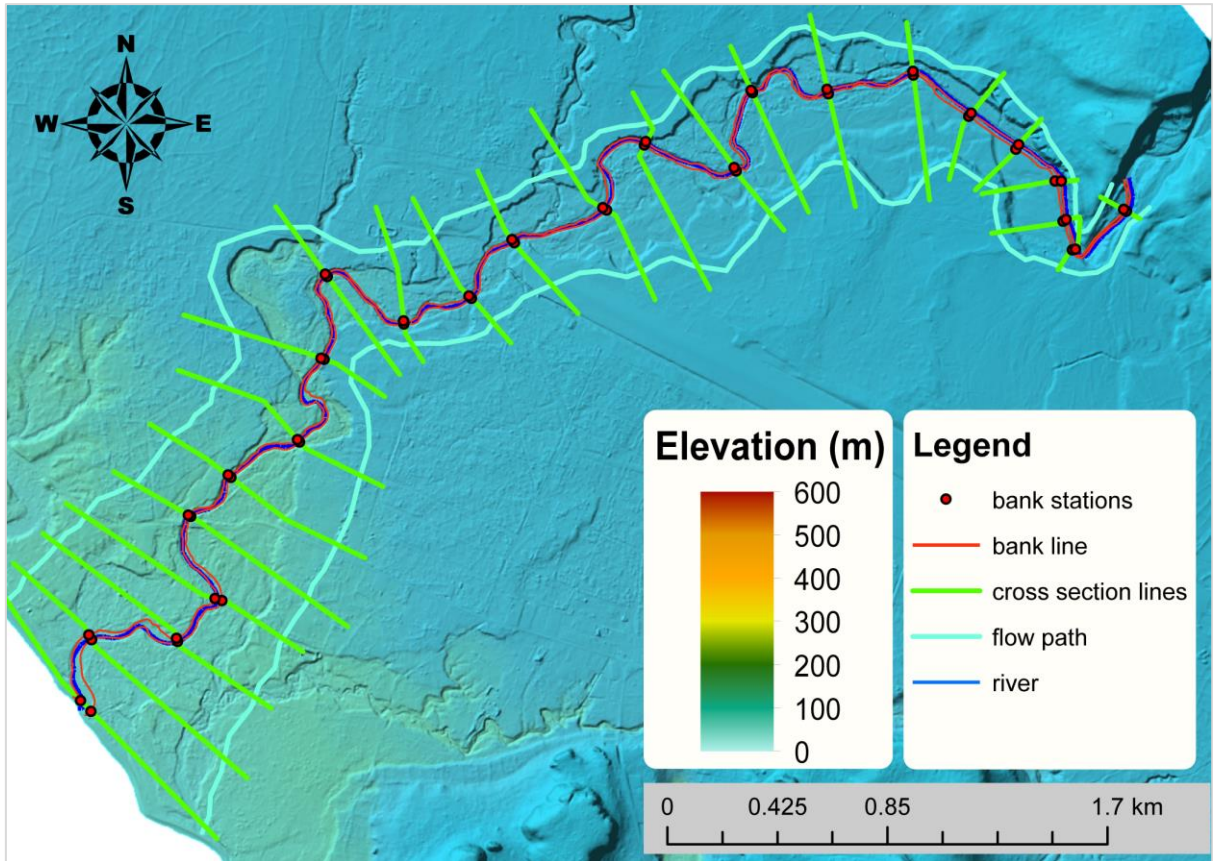
Figure 11. Map showing cross-section measurement sites.
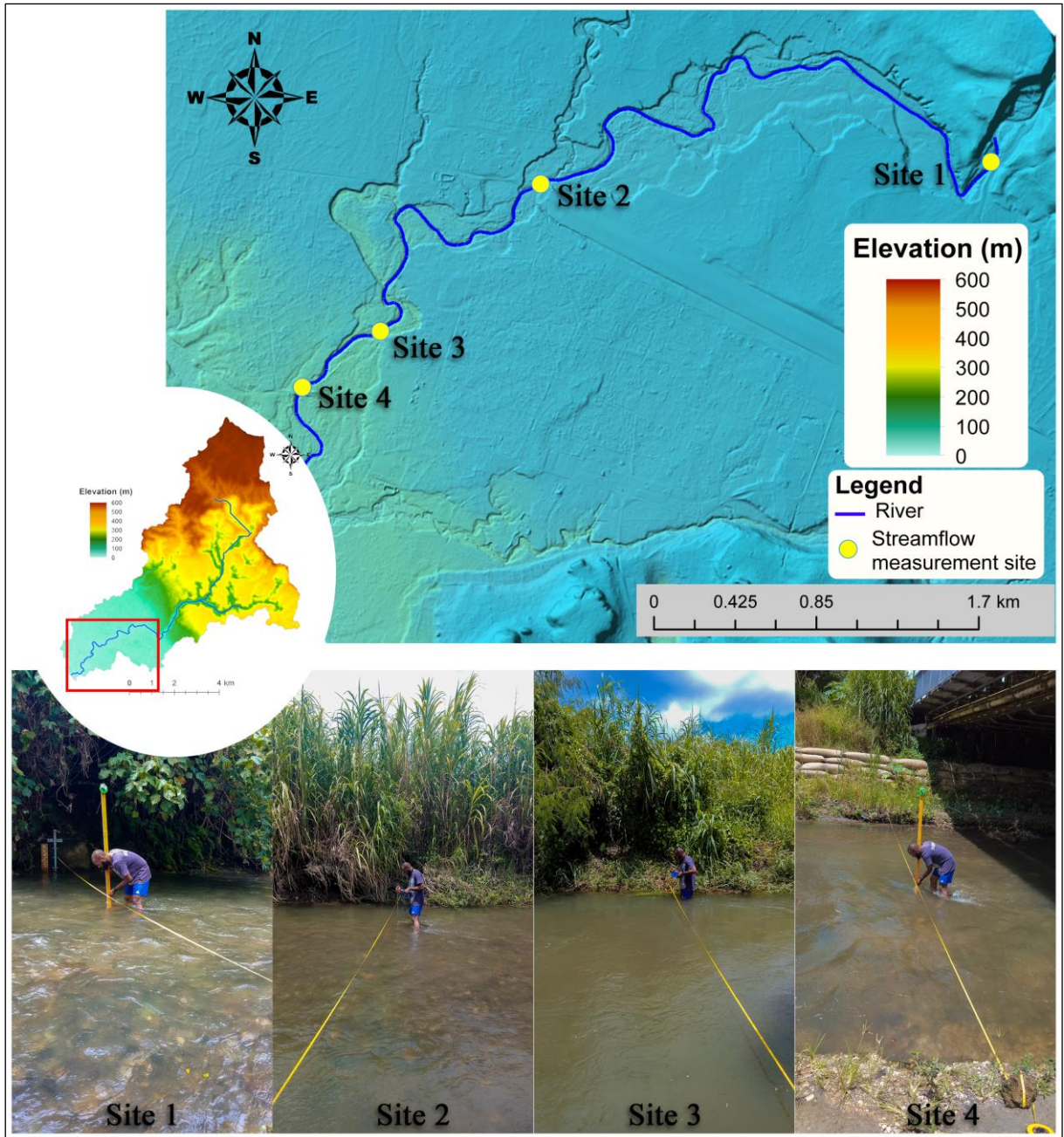
Figure 12. Map of sites where streamflow velocity were measured.
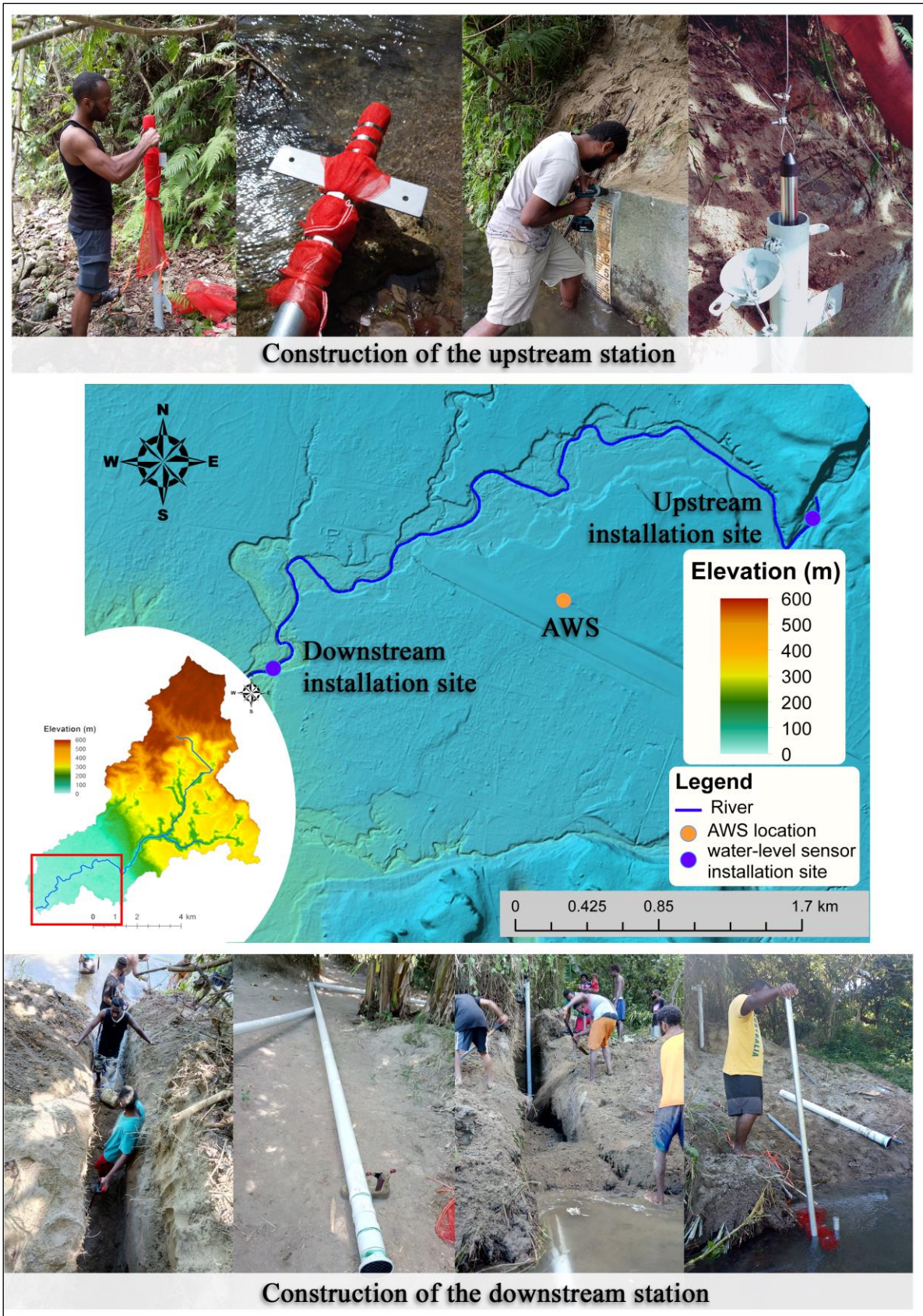
Figure 13. Map of water level data logger installation sites and the AWS location.

Table 2. Discharge measurements during dry and wet season.

Site	Date	Slope	Cross-sectional flow area (m2)	Wetted Perimeter (m)	Hydraulic radius	Discharge (m3/s)	Manning's coefficient
Dry Season Discharge							
1	19/08/15	0.005	2.35	9.15	0.26	1.31	0.05
2	19/08/15	0.002	2.68	14.05	0.19	1.71	0.023
3	19/08/15	0.003	2.36	7.17	0.37	1.44	0.046
4	19/08/15	0.002	2.45	8.88	0.28	1.44	0.032
1	19/08/19	0.005	2.35	9.68	0.24	1.6	0.038
2							
3							
4	19/08/19	0.002	2.55	9.48	0.27	1.43	0.033
Wet Season Discharge							
1	20/03/04	0.005	2.63	8.069	0.33	1.29	0.07
2	20/03/04	0.002	2.65	9.12	0.29	1.38	0.038
3	20/03/04	0.003	3.02	7.32	0.41	1.66	0.055
4	20/03/04	0.002	2.51	10.05	0.25	1.75	0.025
1	20/03/07	0.005	2.59	8.06	0.32	1.52	0.056
2	20/03/07	0.002	2.61	9.11	0.29	1.29	0.039
3	20/03/07	0.003	2.81	7.26	0.39	1.73	0.048
4	20/03/07	0.002	2.43	10.05	0.24	1.52	0.028
1	20/03/10	0.005	2.54	8.06	0.31	1.32	0.063
2	20/03/10	0.002	2.59	9.11	0.28	1.5	0.033
3	20/03/10	0.003	2.77	7.22	0.38	1.65	0.049
4	20/03/10	0.002	2.29	10.05	0.23	1.58	0.024
1	20/03/13	0.005	2.69	8.07	0.33	1.2	0.076
2	20/03/13	0.002	2.7	9.12	0.29	1.45	0.037
3	20/03/13	0.003	3.05	7.32	0.41	1.68	0.056
4	20/03/13	0.002	2.53	10.05	0.25	1.75	0.026

Table 3. TC Pam flood extent coordinates obtained from community members.

Points	Date	Interviewee	Coordinates	
From upstream to downstream				
1	2020/03/08	Mr. Nakou	$168^0 18'14.739"E$	$17^o 41'25.581"S$
2	2019/08/21	Family Nakou	$168^0 18'20.304"E$	$17^0 41'30.197"S$
3	2019/08/21	Mr. Morris	$168^0 17'59.87"E$	$17^0 41'31.362"S$
4	2020/03/08	Mrs. Sandy	$168^0 17'56.483"E$	$17^0 41'38.095"S$
5	2019/08/21	Captain. Rex	$168^0 18'11.215"E$	$17^0 41'39.519"S$
6	2019/08/21	Family William	$168^0 17'44.269"E$	$17^0 41'50.313"S$
7	2019/08/21	Mr. Albert	$168^0 17'55.989"E$	$17^0 41'51.534"S$
8	2019/08/21	Family John M	$168^0 17'29.688"E$	$17^0 42'2.44"S$
9	2019/08/21	Family John M	$168^0 17'46.964"E$	$17^0 42'3.904"S$
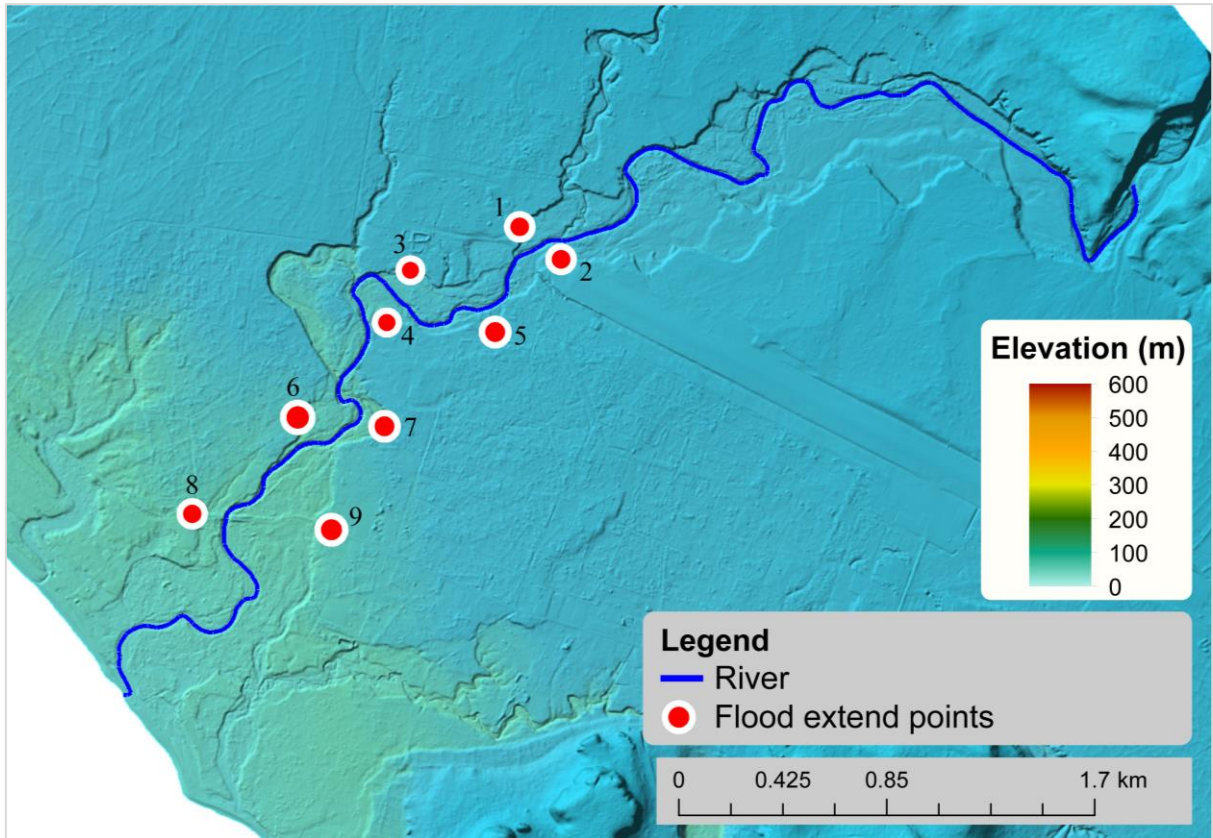
Figure 14. Flood extent points during TC Pam in 2015.

3.3.3 Meteorological dataset

As seen in Table 1, there were two sets of meteorological data used. The first was from 1925 – 2017. This dataset only contained the total daily rainfall (24 hours), where the measurements were done manually. The other set of rainfall data was obtained from an AWS, where the rainfall was recorded every 10 minutes since 2016. With regards to flooding and flood simulation, the AWS data was preferable. However, there were also inconsistencies found on the AWS data, where unavailable data has been observed for prolonged periods. Sometimes it could be for an hour, while other times, it could be for almost a day. For example, there were no data available from 2019/09/07 08:00 till 2019/09/12 09:50; a total of 121 hours of unavailable data. As a result, some of the rainfall-runoff events could not be analyzed.

3.4 Runoff Analysis

It is possible to define runoff as the volume of water released into surface streams. Runoff involves the water that runs across the surface of the ground and into the waterways to enter a stream and infiltration, the water that travels by way of gravity through the soil toward a stream and ultimately empties into the channel. This section explains the mechanism involved in the determination of runoff and the model used in the process.

3.4.1 HEC-HMS Model

As described in the previous chapter, this model includes precipitation, runoff, baseflow, and channel flow modeling with a time-series interval of 30 minutes. Figure 23 shows a representation of the model process used in this study. The factors influencing runoff are normally divided into two groups in a rainfall-runoff relationship: physiographic and climatic factors.

Physiographic features include watershed size, watershed form, watershed slope, watershed orientation, land use, soil moisture, soil composition, topographic and landscape characteristics, and drainage density. Besides, climatic factors include how much precipitation falls, the rate of rainfall, how long the rain falls, and where the rain falls. These factors are captured within the HEC-HMS runoff model. The model utilizes several methods when predicting runoff.

This study uses six methods that are supported by HEC-HMS to manage runoff within the watershed. The simple canopy method, simple surface method, SCS curve number, SCS unit hydrograph, baseflow method, and the Muskingum method. Figure 15 shows the HEC-HMS interface where the methods are determined.
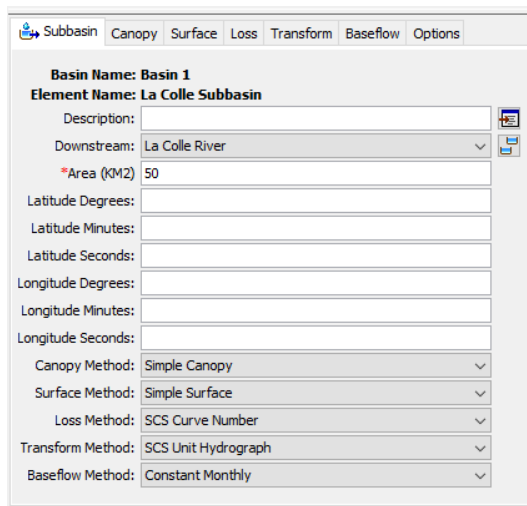
Figure 15. HEC-HMS Methods used in the study.

1. Simple Canopy Method: This method illustrates a basic method of representing a plant canopy. No precipitation intercepted by the canopy falls to the surface before the canopy's storage capacity is exhausted. Once exhausted, additional precipitation falls to the surface or to the soil directly if no other surface type is presented. The canopy's initial condition is specified as the percentage of the canopy's storage capacity containing water at the beginning of the simulation. Figure 16 shows the parameters as determined in HEC-HMS.
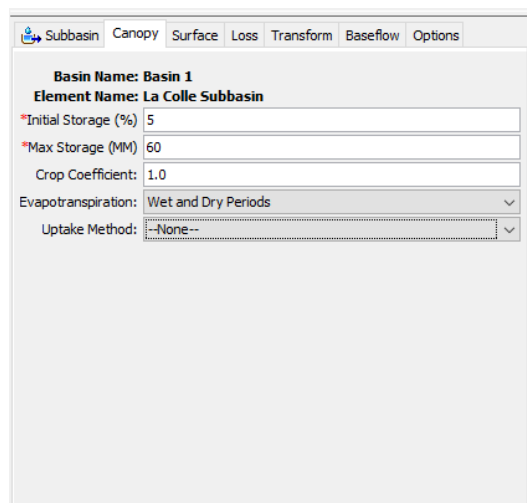
Figure 16. Simple Canopy parameters in HEC-HMS

2. Simple Surface Method: This method is a simple representation of the soil surface. All precipitation type that reaches the soil surface are captured in storage until the surface storage capacity is exhausted. Water that is kept in surface storage also infiltrates into

the soil whenever it is present in storage, even if the storage is not full. When the storage capacity is full, surface runoff is generated. This runoff also happens when precipitation rate exceeds the infiltration rate. Figure 17 shows the surface's initial condition that is specified as the percentage of the surface's storage capacity containing water at the beginning of the simulation.

Figure 17. Simple Surface parameters in HEC-HMS

3. SCS Curve Number: The SCS curve number method determines the approximate runoff amount from a rainfall. This method is designed for a single storm event, where the required data for this method is the rainfall amount and the curve number. The area's hydrologic soil group, land use, treatment, and hydrologic condition determines the curve number. Figure 18 shows the curve number parameter interface along with the impervious value.

Figure 18. SCS Curve Number parameters

4. SCS Unit Hydrograph: This method is used to determine the surface runoff. It describes what happens when water that is not infiltrated or deposited on the watershed surface flows over or under the watershed surface. HEC-HMS determines the hydrograph peak by allowing the user to input the lag time, as seen in Figure 19.
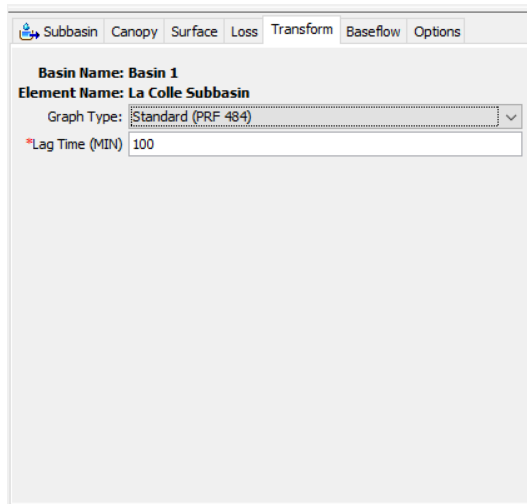
Figure 19. SCS Unit Hydrograph parameters

5. Baseflow Method: This method is used to compute subsurface flow. It simulates the slow subsurface infiltration of water moving from the watershed into the channels. In this study, the parameter was determined by the monthly constant discharge amount. Since monthly constant discharge amounts were used, the spin-up time is covered by the monthly constant depending on which month the simulation begins. Figure 20 shows how monthly constant values are placed in HEC-HMS.
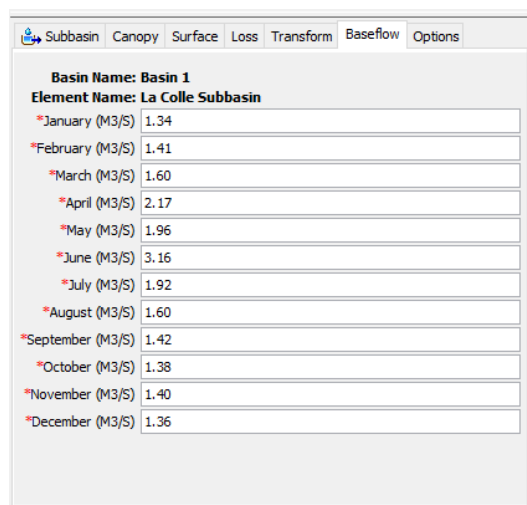
Figure 20. Constant Monthly parameters

6. Muskingum Method: This flood routing method was developed during the 1930s for flood control of the Muskingum River Basin, which is located in Ohio, USA.

This method uses the stored volume at both ends of the reach to become the stage function when the water surface cannot be assumed horizontal, especially during flood events.

Figure 21 shows the different storage components for a given instant in time along a typical reach.
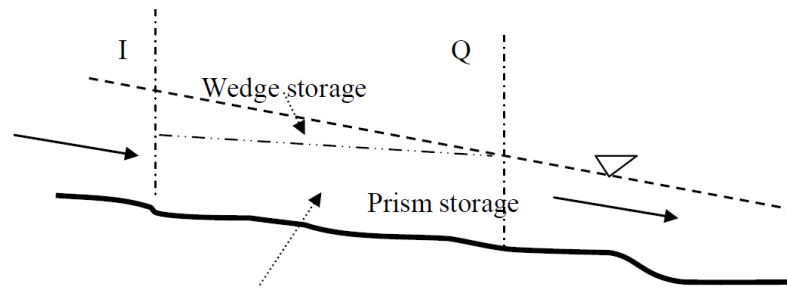
Figure 21. River reach storages

At any given time, the continuity equation holds: $dS/dt = I(t) - Q(t)$ where total storage S is the sum of wedge storage and prism storage. The prism storage S_p is considered a direct function of the storage at the downstream end of the reach and it is the function of the outflow $S_p = f_1(Q)$. The wedge storage S_w exists because the inflow, I, differs from outflow Q and so may be assumed to be a function of the difference between inflow and outflow $S_w = f_2(I-Q)$.

The total storage could be represented by:

$$S = f_1 + f_2(I - Q) \qquad \text{Eqn. 16}$$

Assuming that in Eqn. 16, $f_1(Q)$ and $f_2 (I - Q)$ could be both a linear function, we now have

$$S = bI + (K - b)Q = K\left[\left(\frac{b}{K}\right)I + \left(1 - \frac{b}{k}\right)Q\right] \qquad \text{Eqn. 17}$$

and by substituting $X = b/K$ in Eqn. 17, we get

$$S = K[XI + (1 - X)Q] \qquad \text{Eqn. 18}$$

X is a weighting factor indicating how much I and Q contribute to storage in and within the reach length. X values range from 0 to 0.5, while most rivers have an X value between 0.1 and 0.3. K is the time parameter; it is the flood wave travel time through the channel reach. The Muskingum method routing equation is derived by combining Eqn. 16 and Eqn. 18. Figure 22 shows the routing parameter interface.
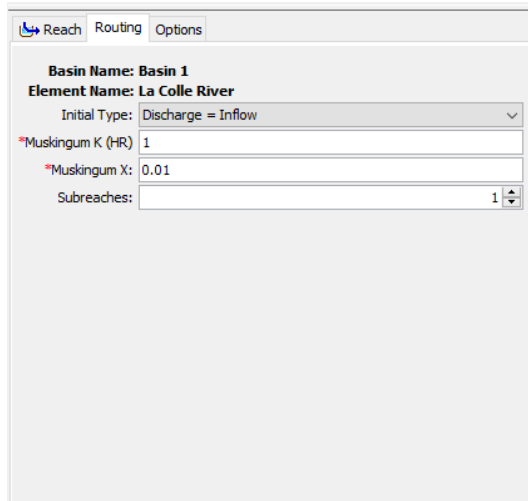
Figure 22. Muskingum routing method parameters

Based on the discussed methods, calibration of the model was done by adjusting each of the methods' parameters. Listed in Table 4 are each of all the method's parameters that have been adjusted when analyzing 13 rainfall-runoff events against observed discharge data.
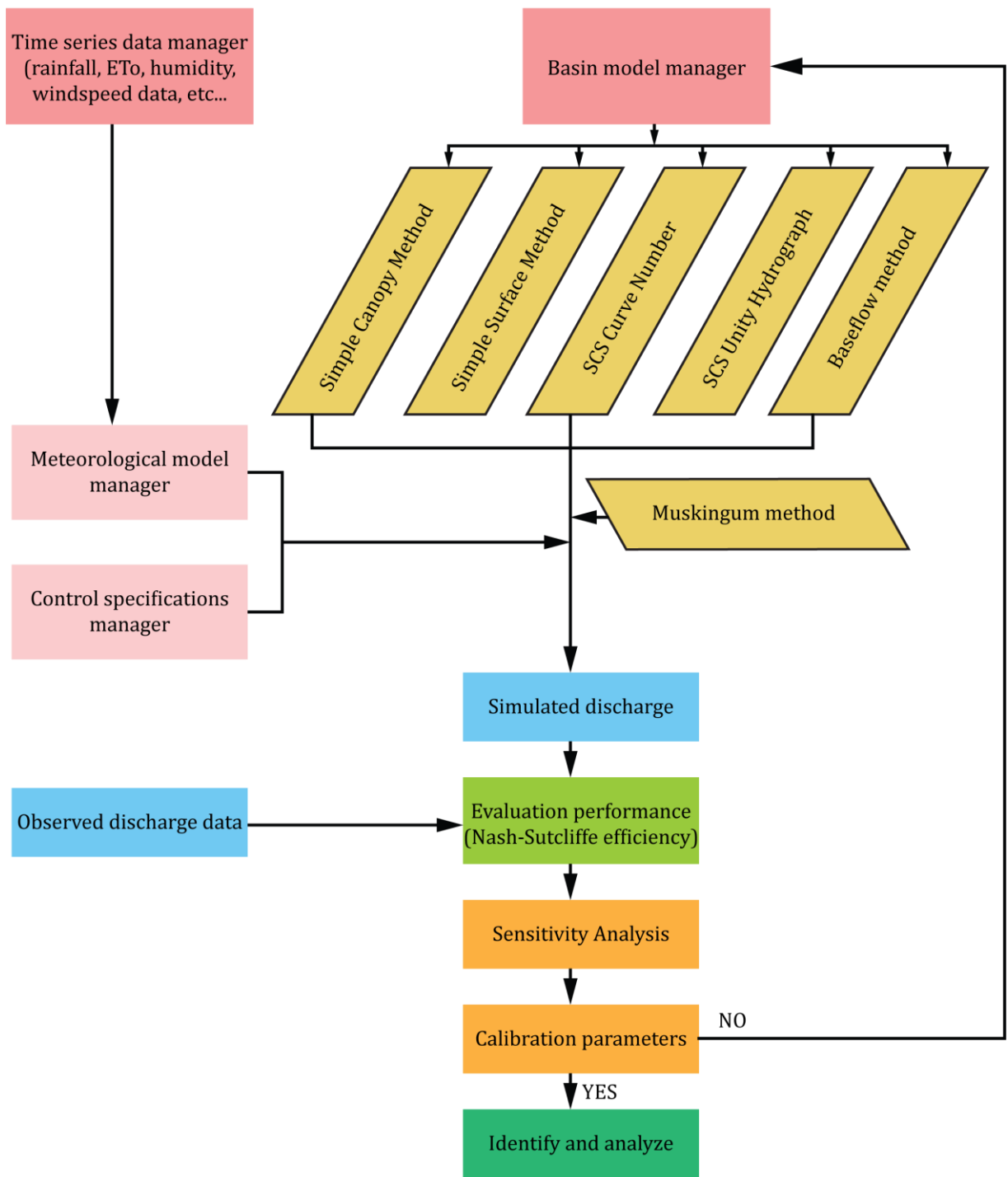
Figure 23. Representation of the HEC-HMS specific to this study.

Table 4. Calibrated parameter list and values

Parameters	Units	Range
Canopy		
Initial storage	%	0 – 100
Max storage	mm	0 – 1500
Crop Coeff.	constant	0 – 1
Surface		
Initial storage	%	0 – 100
Max storage	mm	0 – 1500
Loss		
Initial abstraction	mm	0 – 500
Curve Number	constant	30 – 77
Impervious	%	0 – 100
Transform		
Graph type	Standard	
Lag time	Min	18 – 616
Baseflow		
Constant monthly	m^3/s	1.34 – 2.76
Routing		
Muskingum K	HR	1 – 3.5
Muskingum X	constant	0.0 – 0.5

3.5 Flood Simulation

Flood simulation was done in HEC-RAS, both on the original and the modified terrain. However, the modified terrain was produced in RAS Mapper – a HEC-RAS extension. This section details the processes involved in the simulation.

3.5.1 HEC-RAS Model

HEC-RAS was selected as the model to be used in this study apart from other models such as Sediment and River Hydraulics – 2D, Center for Computational Hydroscience & Engineering 2D-Flow, IBER, MikeUrban, Mike 11 and Mike 21. Observation results of the watershed, study area, and hydrological data availability concluded HEC-RAS is the model choice. As Azouagh and Hilal (2018) stated, HEC-RAS performs well in rivers with a low gradient and in remote areas where data is limited.

Figure 24 shows the HEC-RAS workflow procedure used in this study, where initial geometric data used in HEC-RAS were prepared in ArcGIS, using the HEC-GeoRAS GIS extension. With regards to the purpose of this study, the prepared geometric data includes stream centerline, river bank lines, flow paths, and stream cross-section lines. Geometric data are then exported from ArcGIS by generating the RAS GIS import file (.RASImport.sdf).

In HEC-RAS, the stream centerline is often referred to as the river. It is obtained by drawing a line from the upstream to the downstream of the river on the river channel's center. The bank lines are the lines determining the river edge along the river channel. There are two bank lines, one on the left and the other on the right bank. Flow paths are lines that are used to compute reach length between two cross-sections on the left and right overbank. Creating a flow path in the main channel is not necessary in HEC-RAS. Figure 11 shows the mentioned geometric data created along La Colle river.

The RAS GIS file is then imported into HEC-RAS for computational analysis. After the flow data and Manning's value are added, computations were executed. Obtained results based on the original terrain were then analyzed and verified. After verification and calibration, computations were then applied on the modified terrain. Inundated boundaries (shapefiles) are then imported back into ArcGIS for the inundated area size determination.

Spin up period of 12 months was used in this study based on observed discharge with a time interval of 30 minutes. However, final simulations are performed with a time interval of 60 minutes. This is because the rainfall return periods were obtained from a dataset with hourly rainfall reading.

3.5.2 Terrain modification

Terrain modification was done in RAS Mapper. Modification details regarding extraction depth were obtained through field investigation before and after sand extraction activity, while the researcher and DOWR selected the potential extraction sites.

Before and after sand extraction activity, field investigations revealed that the extraction depth was approximately −1 m from the current stream depth. Because of a short and temporary sand extraction permit issued by the government to the extraction companies, other potential extraction sites were chosen should the current site is temporarily closed due to unforeseen environmental issues. The two potential sites were selected based on streamflow velocity and the terrain topography. As determined by DOWR investigations, streamflow velocity was suitable for the deposition of sediments between sites 1 and 3. Further upstream, the velocity would not allow for fine sediment deposits. Sites 2 and 3 are also easy to access; thus, sand transportation would be much easier. Figure 25 shows the location of sand extraction sites 1, 2, and 3. Site 1 is where sand is currently extracted, sites 2 and 3 are the potential extraction sites.

Extraction sites were modified by widening the riverbanks and deepening the streamflow area. On the selected sites, the channel was deepened to a depth of −1, −2, and −3m from the current stream channel depth.
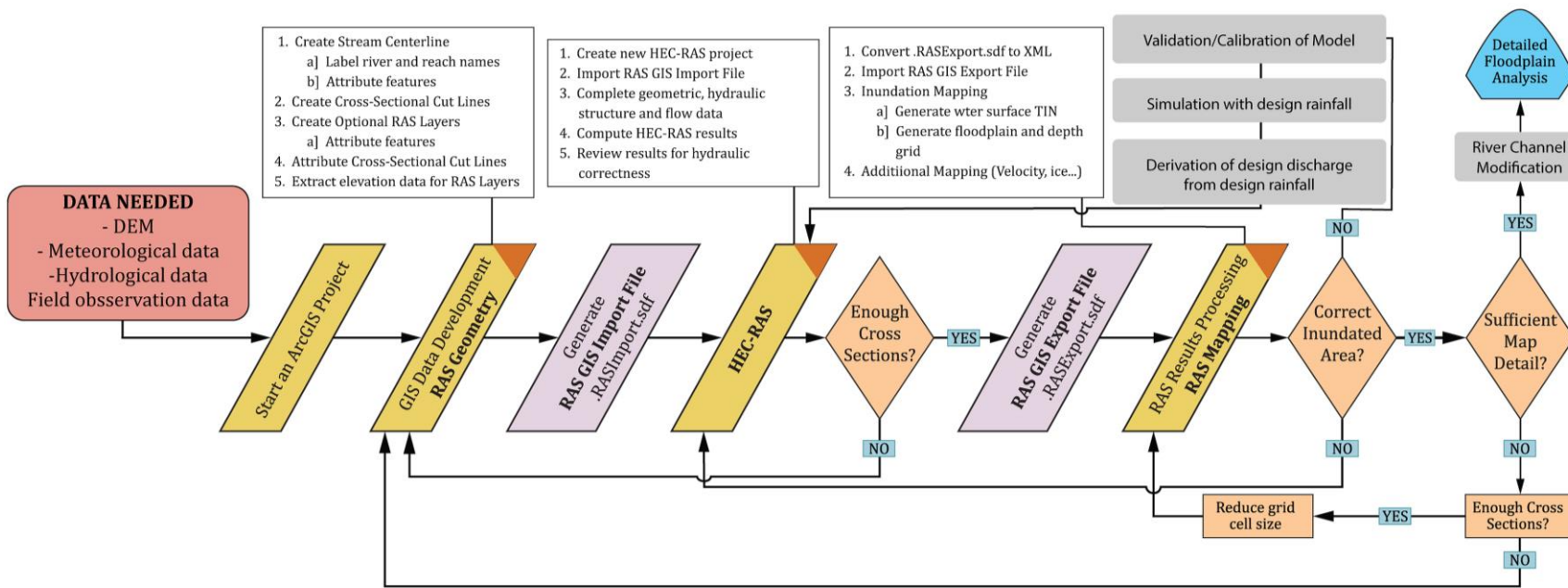
Figure 24. Representation of HEC-RAS workflow.

DATA NEEDED
- DEM
- Meteorological data
- Hydrological data
- Field obsservation data

Box 1:
1. Create Stream Centerline
   a] Label river and reach names
   b] Attribute features
2. Create Cross-Sectional Cut Lines
3. Create Optional RAS Layers
   a] Attribute features
4. Attribute Cross-Sectional Cut Lines
5. Extract elevation data for RAS Layers

Box 2:
1. Create new HEC-RAS project
2. Import RAS GIS Import File
3. Complete geometric, hydraulic structure and flow data
4. Compute HEC-RAS results
5. Review results for hydraulic correctness

Box 3:
1. Convert .RASExport.sdf to XML
2. Import RAS GIS Export File
3. Inundation Mapping
   a] Generate wter surface TIN
   b] Generate floodplain and depth grid
4. Additiional Mapping (Velocity, ice...)

Validation/Calibration of Model

Simulation with design rainfall

Derivation of design discharge from design rainfall

Detailed Floodplain Analysis

River Channel Modification

Process boxes (left to right):
- Start an ArcGIS Project
- GIS Data Development **RAS Geometry**
- Generate **RAS GIS Import File** .RASImport.sdf
- **HEC-RAS**
- Enough Cross Sections?
- Generate **RAS GIS Export File** .RASExport.sdf
- RAS Results Processing **RAS Mapping**
- Correct Inundated Area?
- Sufficient Map Detail?

Decision labels: YES, NO

- Reduce grid cell size
- Enough Cross Sections?

Figure 25. Sand extraction location within the watershed

3.6 Summary

The study methodology outlined in this chapter includes explanations on the research design, research dataset, field observation and investigation, hydrological dataset, meteorological dataset, runoff analysis, HEC-HMS, flood Simulation, HEC-RAS, and terrain modification. The next chapter discusses the obtained results.

CHAPTER FOUR: RESULTS and DISCUSSION

4.1 Introduction

The research was conducted to achieve the three main objectives stated in section 1.4, in line with the aim, as indicated in section 1.3. The hydrological field investigations, the hydrological and meteorological data analysis, and finally, the simulated flood results will be addressed in this chapter.

4.2 Field observation data analysis

The three cross-section measurements obtained to verify the LiDAR DEM show that the DEM is accurate and can be used in the study. The NSE coefficient for sites 1, 2, and 3 shows an average NSE coefficient of 0.926. Therefore, the LiDAR DEM can be said to represent the study area topography accurately. Figure 26(a) refers to site 1 while (b) refers to site 2, and (c) refers to site 3. Figure 26 compared field cross-section measurements and the LiDAR DEM cross-section, while Figure 27 shows the three sites' NSE coefficient.

As shown in Table 2, the Manning's roughness coefficient was obtained from 21 streamflow measurements. Upstream of La Colle river has an average Manning's coefficient of 0.063 while 0.028 on the downstream. Obtained results also show a 1.9 % increase in wet season discharge compared to dry season discharge: meaning, a somewhat constant discharge amount during the two seasons.
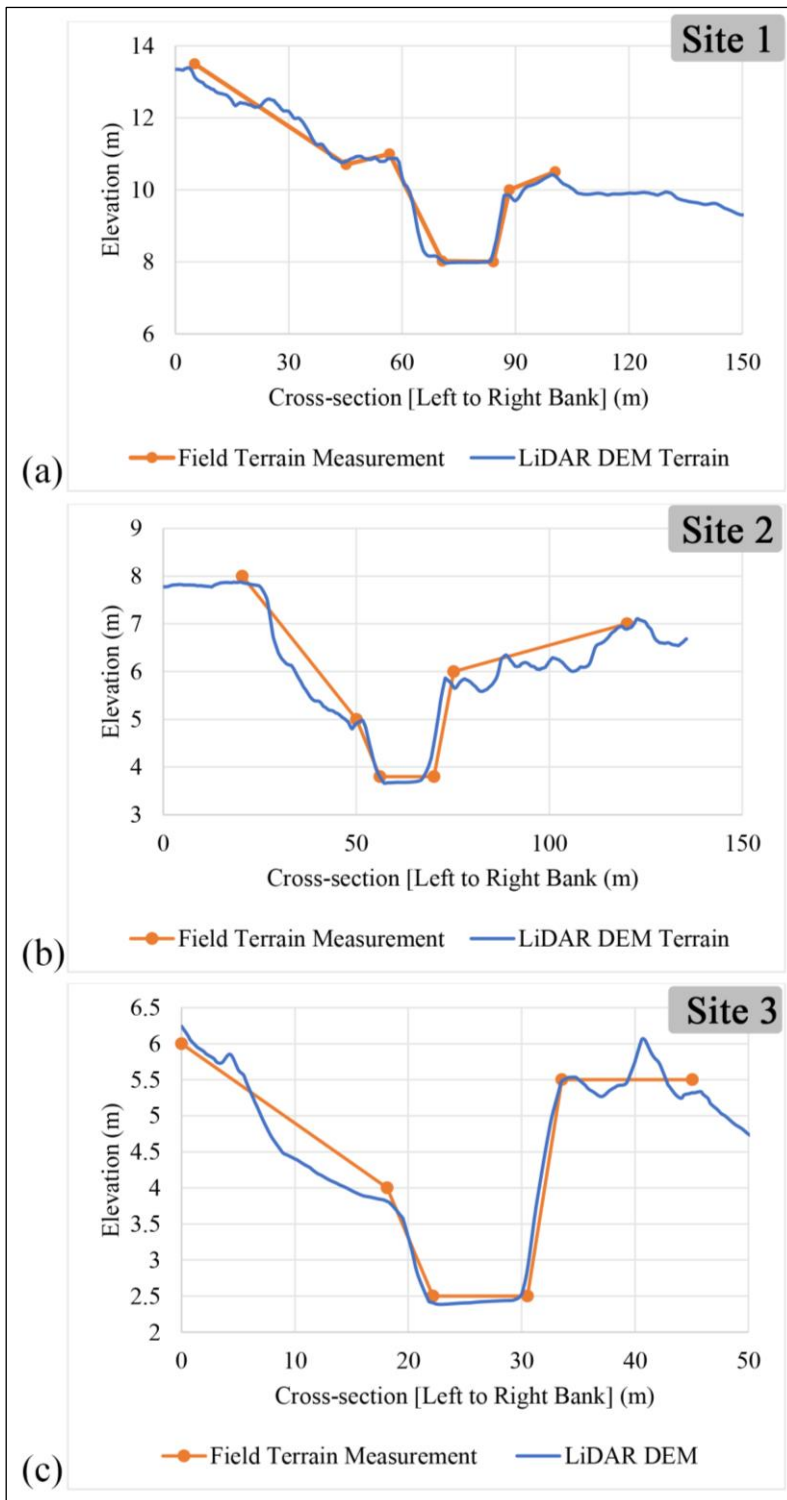
Figure 26. Comparison graphs of measured cross-sections and LiDAR DEM cross-sections.
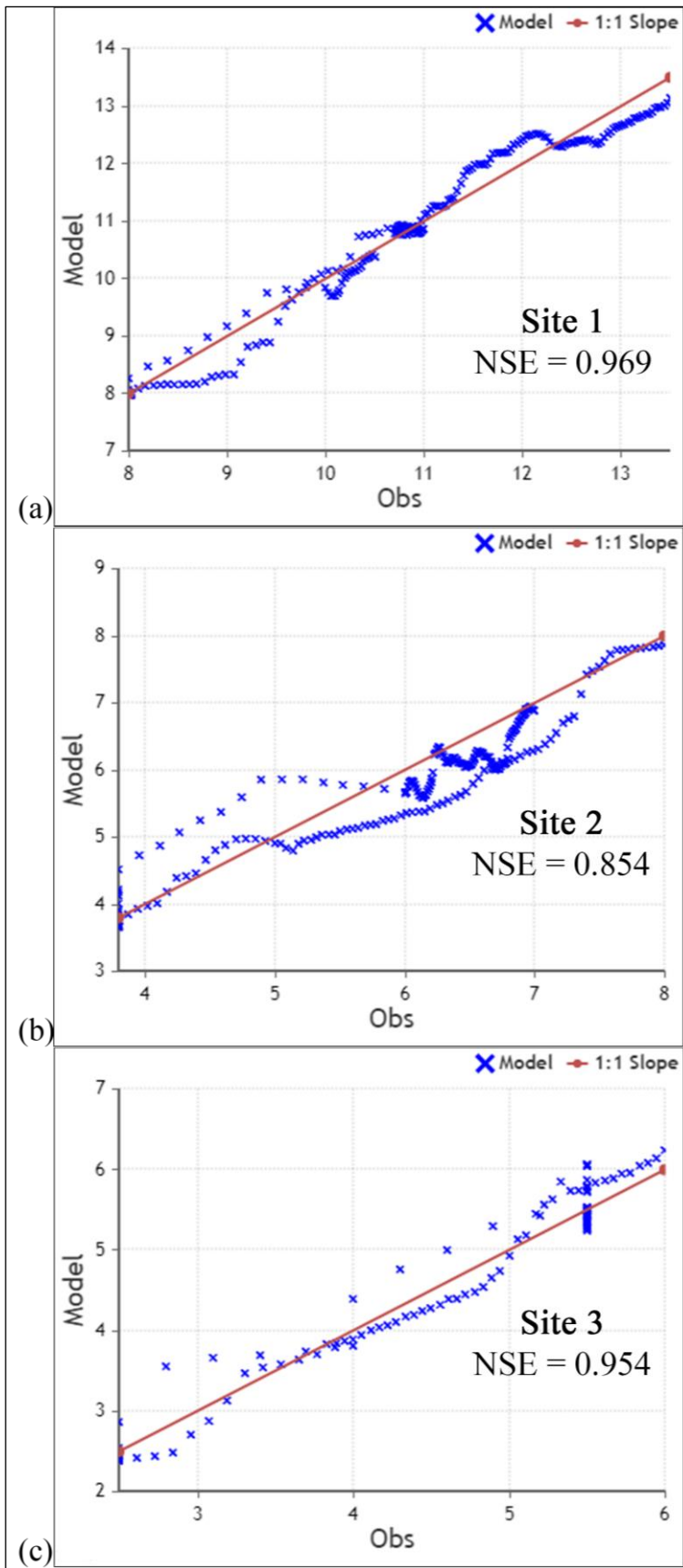
Figure 27. NSE's relative magnitude of field measurements compared to LiDAR DEM data.

4.3 Hydrological data analysis

As listed in Table 3, obtained data from local community members on TC Pam's flood extent was then plotted in ArcGIS. Based on TC Pam's rainfall amount, flood was simulated, and the results were compared to flood-extent points given by the community. The result shows a correlation between flood simulation extent and points provided by the community.

It must be noted that the interview was done in 2019, while TC Pam occurred in 2015. The chances are high that community members might provide incorrect flood extent points. For example, in Figure 28, point number 5 was further away from the simulated flood extent.

With regards to TC Pam's discharge data, the simulated result could also be underestimated as part of the rainfall data was unavailable: due to strong winds preventing observers from going outside to collect rainfall data.

Figure 28 also verified the calibrated parameters in Table 6. Even though the calibrated parameters have a NSE coefficient of 0.35 as seen on Figure 36, the outcome seemed accurate.
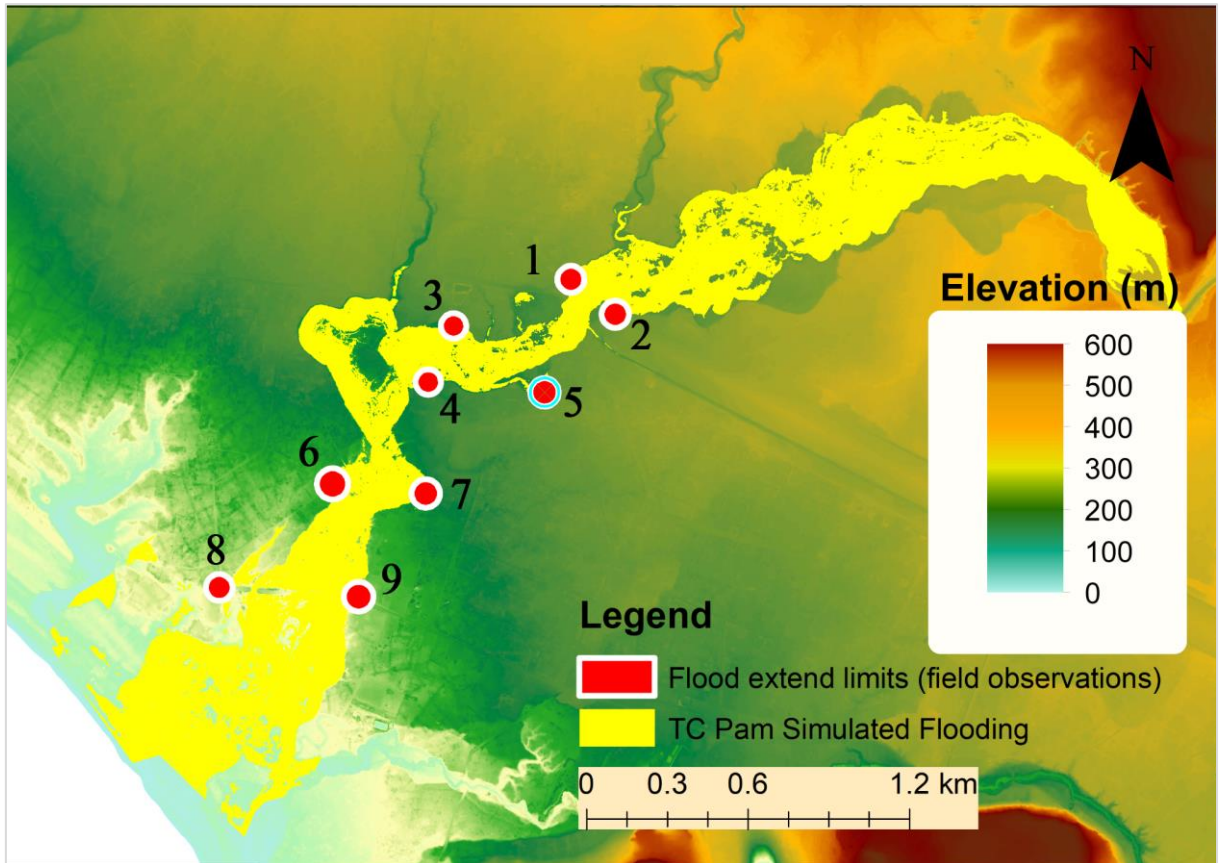
Figure 28. Map of obtained flood extent points and TC Pam flood simulation.

4.4 Meteorological data analysis

Thirteen rainfall events were selected and analyzed in this study, and the results are shown in Table 5. The analyzed events occurred between August 2019 and December 2020. There were no extreme events with larger rainfall amounts within the timeframe that could result in flooding. Analysis of the rainfall events resulted in the determination of lag time between peak rainfall and peak runoff. The analyzed lag time between peak rainfall and peak upstream discharge ranges from 0.3 hours to 5.2 hours, with an average of 2.6 hours. Peak discharge lag time between upstream and downstream station ranges from 2 hours to 3.5 hours, with an average of 3 hours.

4.5 Return rainfall period analysis

Rainfall return periods of 10- 50- and 100-years were determined using meteorological data from 1985 to 2019. Figure 29 shows the Line graph expression that was used to determine the return rainfall amount. For the 10-year return period, a total of 424mm is projected, 670.92mm for the 50-year return period, and 777.23mm for the 100-year return period. Rainfall pattern used in all simulations were generated using TC Harold's rainfall pattern: which made landfall on April 6th, 2020. Figure 32 shows TC Harold's rainfall pattern.

4.6 Rainfall and runoff analysis

Based on the analysis of 13 rainfall events, as shown in Figure 30 and Figure 31, runoff amounts were determined. These 13 events were divided into two groups; Group 1 comprises of events with total rainfall below 50mm/24 hour while events with rainfall greater than 50mm are in Group 2 (only three events). Using HEC-HMS, runoff was determine based on calibrated parameters of Group 2 events. The calibrated parameters are listed in Table 6. The calibrated result was then verified by another rainfall event on December 07th, 2020.

Figure 33(a) shows the calibrated parameters being applied to a rainfall event of less than 50mm/24 hours and Figure 33(b) shows the NSE coefficient of the observed and simulated discharge. With an NSE coefficient of -2.898, the calibrated parameters do not perform well on smaller rainfall events.

Figure 34 and Figure 35 show the calibrated parameters being applied to more than 50mm/24 hours of rainfall events. While Figure 34 has an NSE coefficient of 0.666, Figure 35 has 0.734. This shows that the calibrated parameters performed well with larger rainfall events.

However, when validating the calibrated parameters on a recent rainfall event on December 07th, 2020, there are few things to note. First, the peak timing, the result shows a good correlation between the observed and the calibrated parameters. Second, peak discharge amount, there is also a good correlation between the observed and the calibrated parameters.

However, the NSE coefficient for the calibrated parameters was 0.35. This can be seen in Figure 36. A closer look at the observed discharge in Figure 36 shows that the observed discharge had two peaks while there were no two separate observed peak rainfall times. A possible reason why there are two peaks in the observed discharge could be because of unobserved extra rainfall activity further upstream of the river: since there is only one AWS and it is located further downstream of the watershed. The other possible reason could be due to observed discharge calculation error. On the other hand, Figure 37 shows another recent analysis on a rainfall event on January 26th, 2021, where the graph shows yet another twin peak discharge during the event despite a single rainfall peak. The event has an NSE coefficient of 0.819, much better than the previous validation of the used parameters. As such, it can be concluded that La Colle's watershed could have a large storage capacity. This led to the first peak relating to a quick surface runoff while the second peak is observed after the watershed's storage capacity is exhausted. This validation concluded that the determined parameters can be used for flood simulations with larger rainfall amounts: greater than 100mm of rainfall in 24 hours.

The peak discharge amount for the flood return-periods was determined based on the calibrated parameters, the return-period rainfall amount, and TC Harold's rainfall pattern. Figure 38 shows that for the 10-, 50-, and 100-years flood return period, a peak discharge of 150 m^3/s, 184.2 m^3/s, and 408.8 m^3/s is expected, respectively.

Table 5. Rainfall-runoff analysis results

Event	Beginning of Event	End of Event	Total Rainfall (mm)	Peak rainfall (mm/10mins)	Rainfall Duration (hr)	Total Discharge (m³/s)	Peak Discharge (m³/s)	Discharge Duration (hr)	Upstream Lag time (hr)
1	12/20/2019 5:00	12/20/2019 14:00	36	11.7	4	437,400	2.1	9	0.3
2	1/10/2020 7:00	1/10/2020 14:00	11	9.5	1.5	151,200	0.7	6	3
3	1/11/2020 10:10	1/12/2020 4:48	33.5	8.5	9	1,251,720	0.8	19	3.5
4	2/8/2020 0:05	2/8/2020 14:18	47.5	24.5	5.5	786,240	1.4	14	5.2
5	2/9/2020 23:00	2/10/2020 18:18	55.5	8.5	7	3,552,120	3.7	19.5	3.1
6	3/2/2020 2:40	3/2/2020 15:47	32	19.95	1.5	824,760	1.5	13.5	1.7
7	3/11/2020 13:10	3/12/2020 3:47	34.5	18	2	824,760	0.8	14.5	2.8
8	3/25/2020 12:30	3/26/2020 16:17	56.5	11	4.5	4,132,800	2	28	3
9	3/28/2020 6:30	3/29/2020 9:47	76.5	25.5	9	15,830,100	31.1	27.5	2
10	3/29/2020 10:00	3/30/2020 14:47	46	7.5	7	7,693,920	11.8	19.5	2.5
11	4/2/2020 20:00	4/3/2020 15:17	30	3	9	1,418,040	0.8	19.5	4.1
12	4/6/2020 13:30	4/7/2020 16:17	49.5	3.5	13.5	2,743,200	1.3	20	0.3
13	4/16/2020 14:30	4/17/2020 04:30	2	1.5	1	229,680	0.8	14.5	3
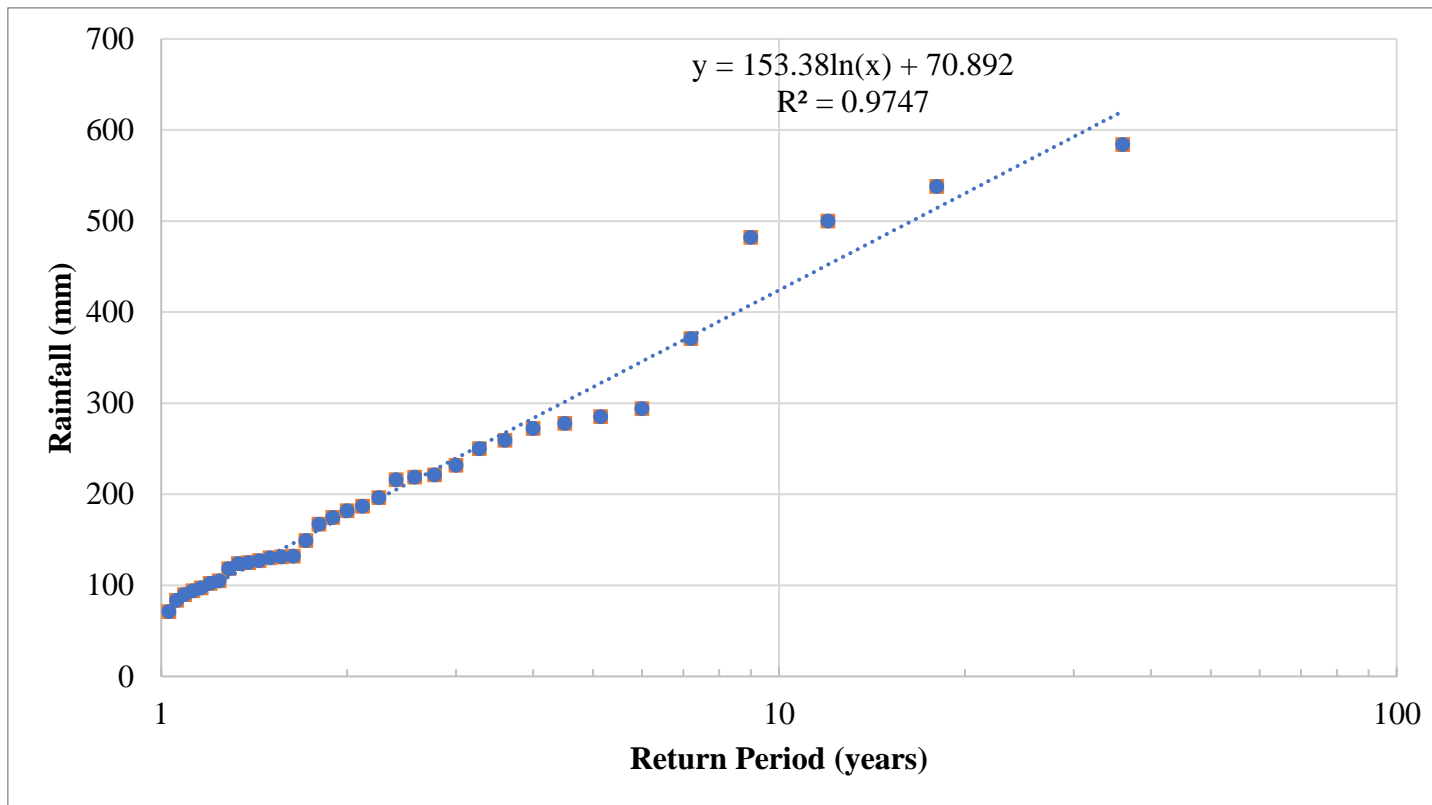
Figure 29. Line graph expression used to determine the return rainfall amount.
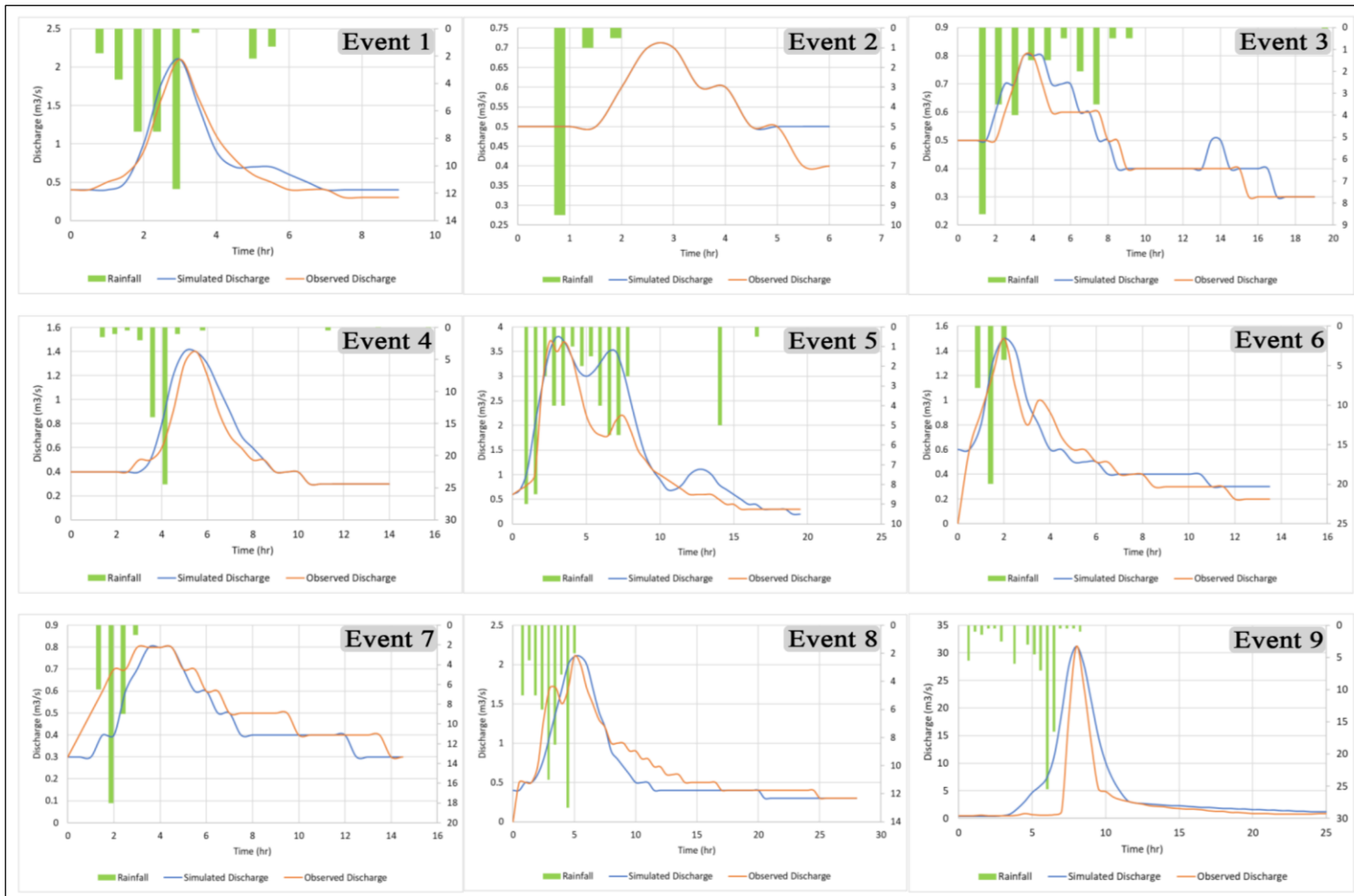
Figure 30. Determination of the calibrated parameters from events 1 to 9.
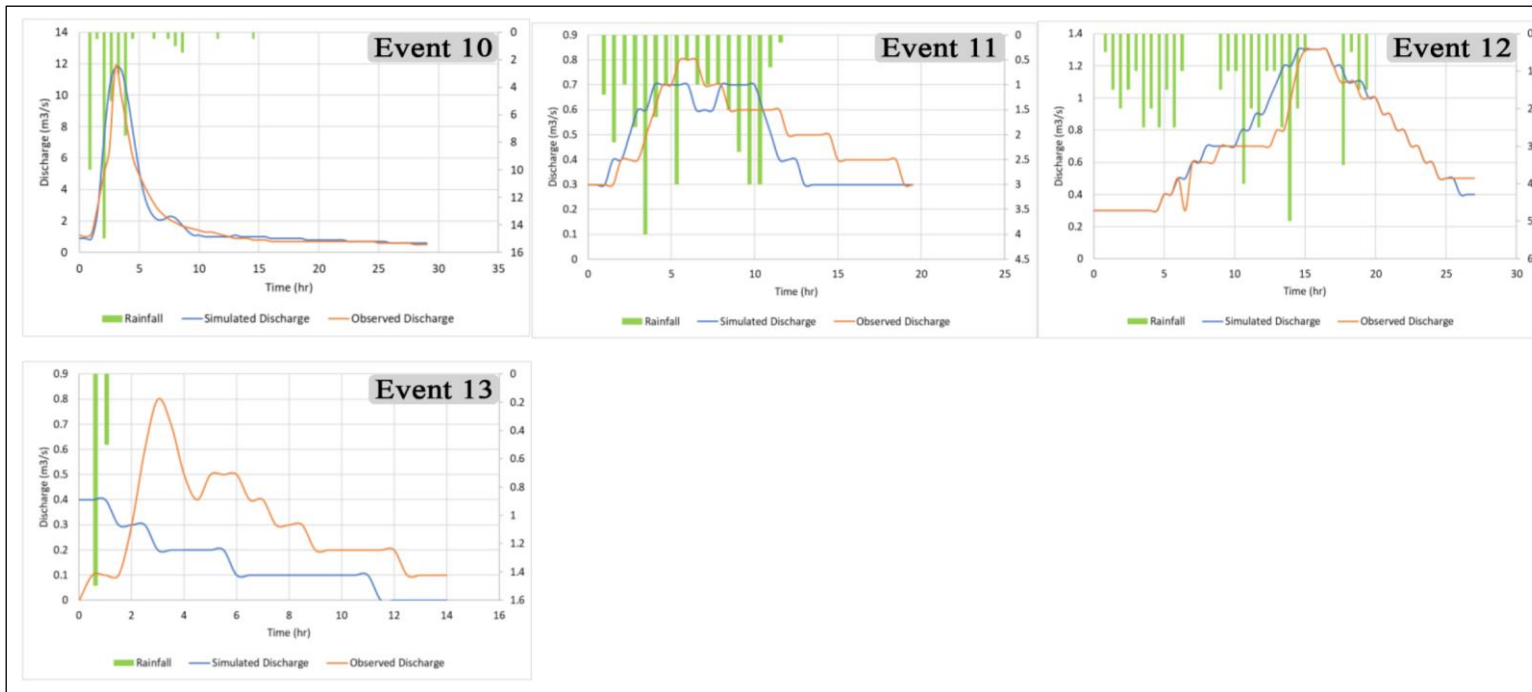
Figure 31. Determination of the calibrated parameters from events 10 to 13.

Table 6. Calibrated parameters from rainfall-runoff events.

Parameters	Units	Range	Calibrated Parameters
Canopy			
Initial storage	%	0 – 100	5
Max storage	mm	0 – 1500	60
Crop Coeff.	constant	0 – 1	1
Surface			
Initial storage	%	0 – 100	10
Max storage	mm	0 – 1500	100
Loss			
Initial abstraction	mm	0 – 500	50
Curve Number	constant	30 - 77	35
Impervious	%	0 – 100	13
Transform			
Graph type	Standard		
Lag time	Min	18 - 617	100
Baseflow			
Constant monthly	m^3/s	1.34 – 2.76	Varies
Routing			
Muskingum K	HR	1 – 3.5	2.1
Muskingum X	constant	0.0 – 0.5	0.3
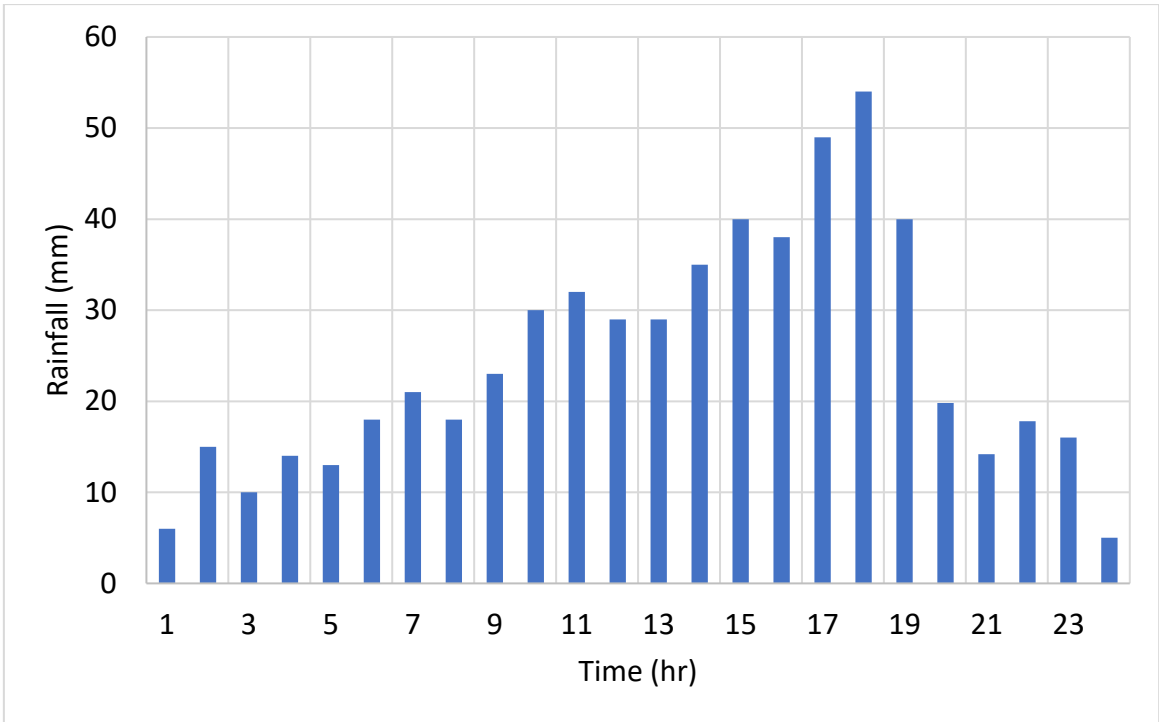
Figure 32. TC Harold rainfall pattern (2020/04/03).
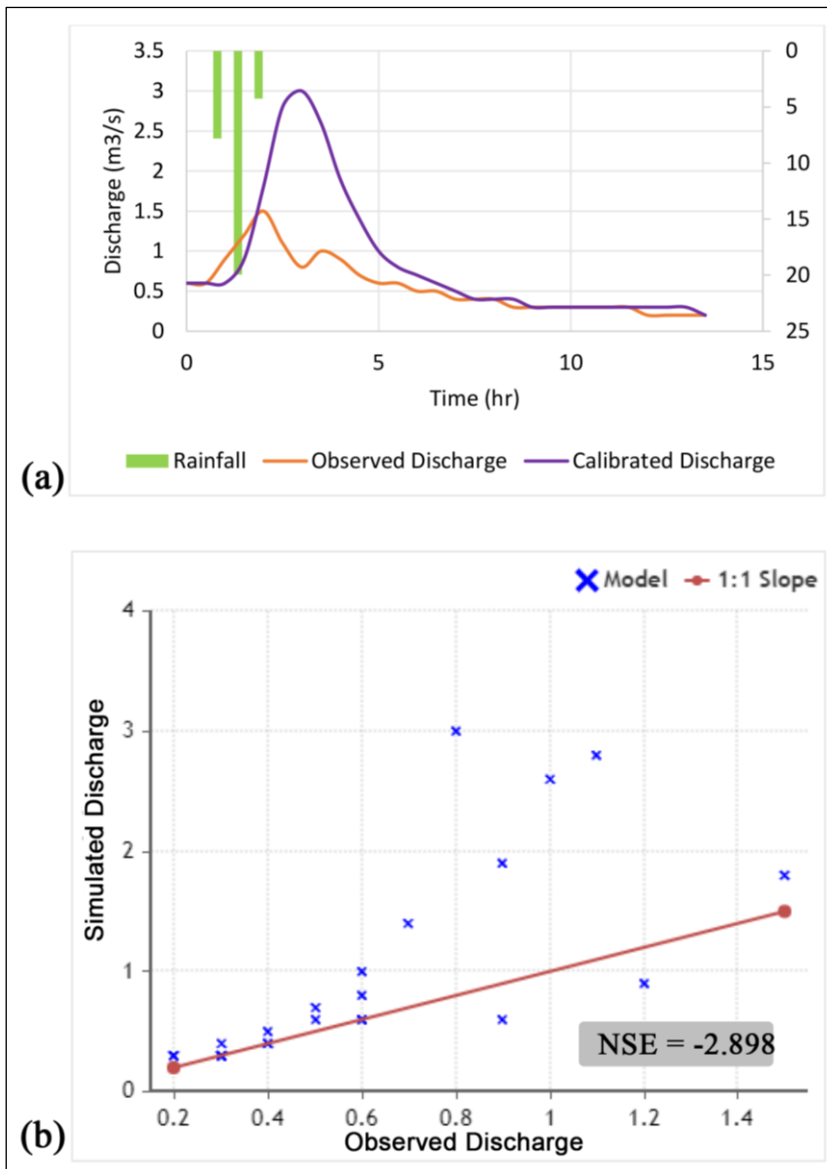
Figure 33. Calibrated parameters being applied on Event 6 and its NSE coefficient.
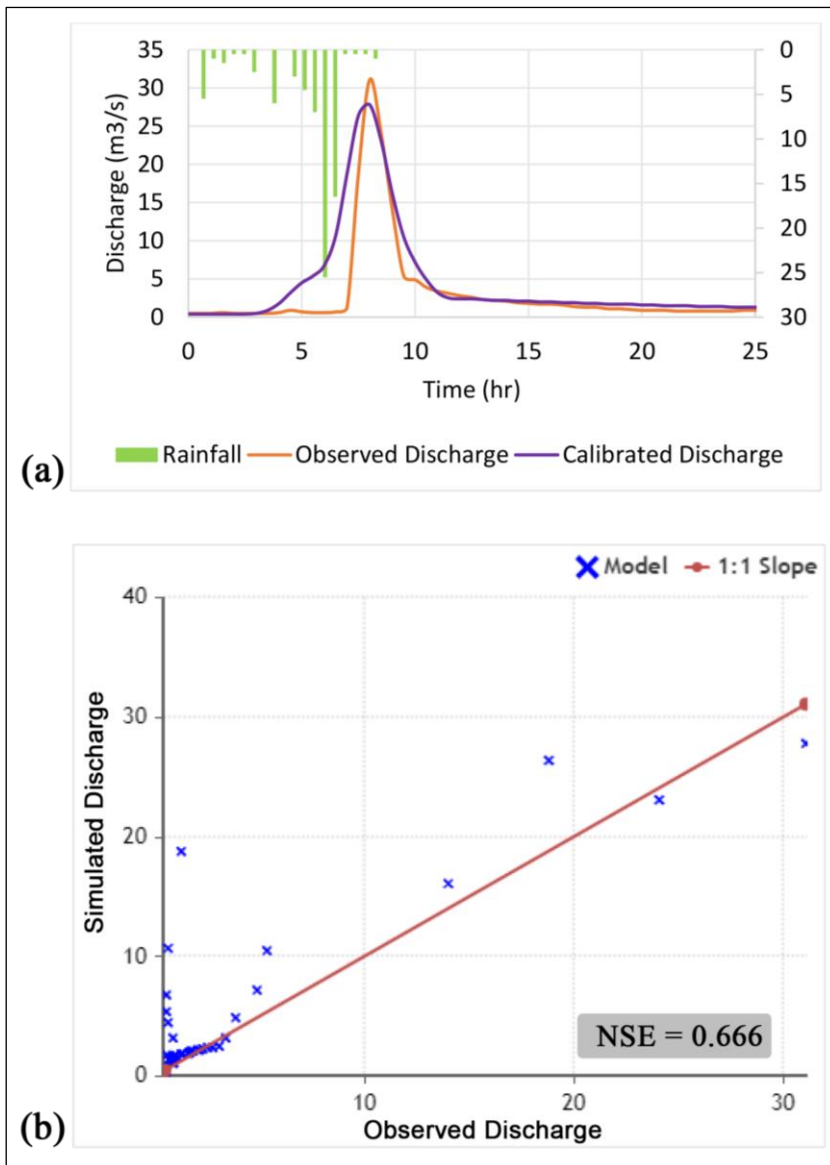
Figure 34. Calibrated parameters being applied on Event 9 and its NSE coefficient.
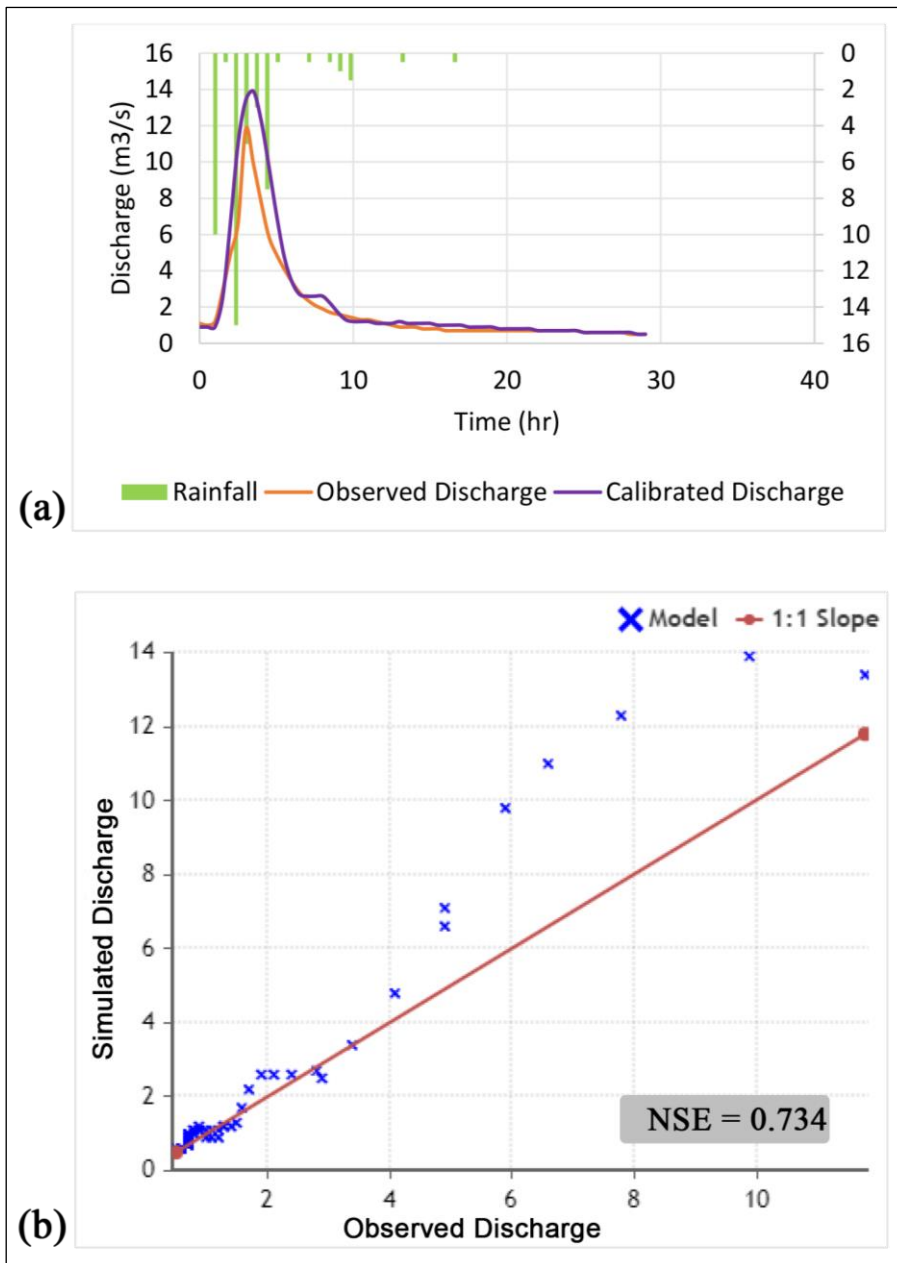
Figure 35. Calibrated parameters being applied on Event 10 and its NSE coefficient.
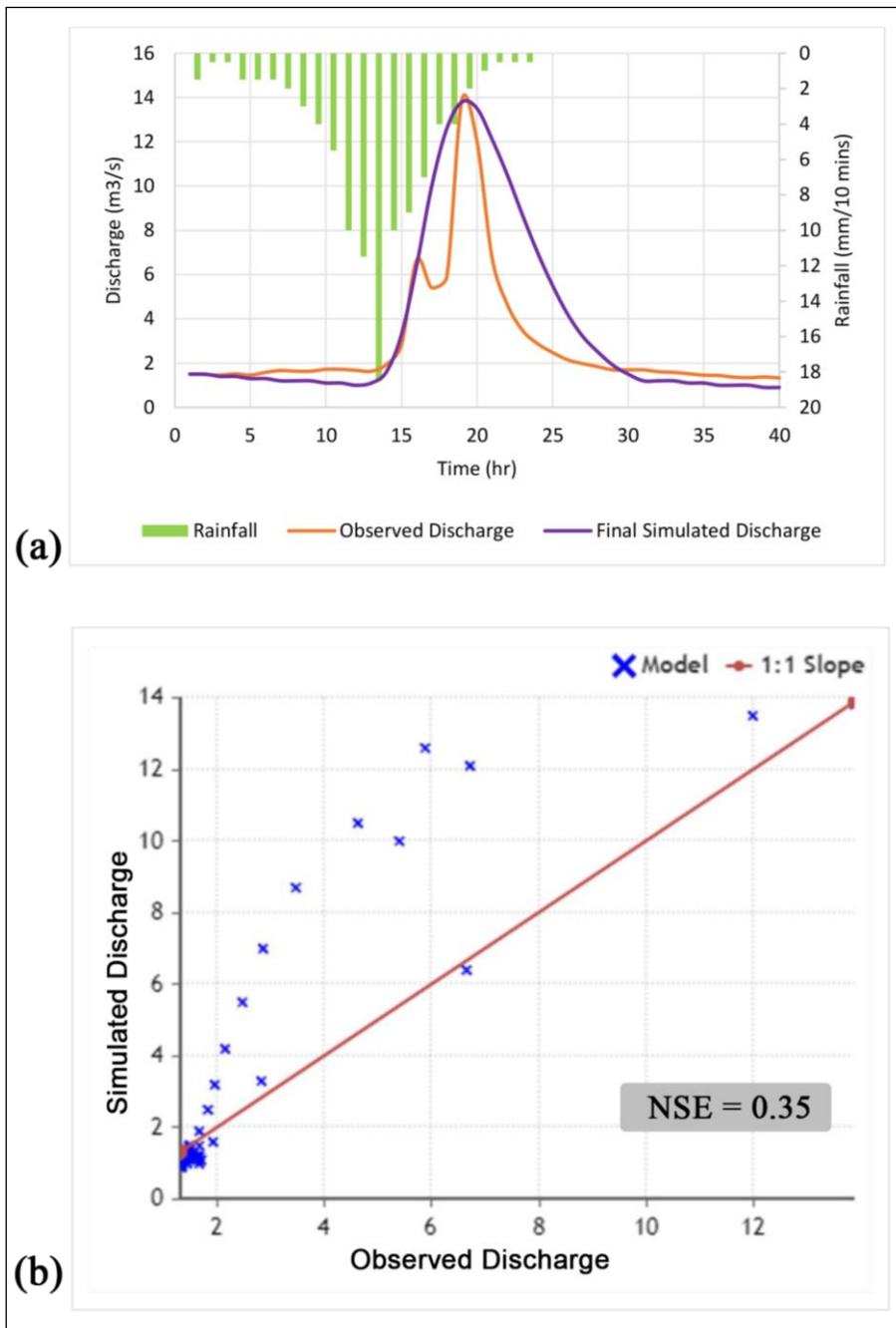
Figure 36. Validation of the calibrated parameters based on the 2020/12/07 rainfall event and its NSE coefficient.
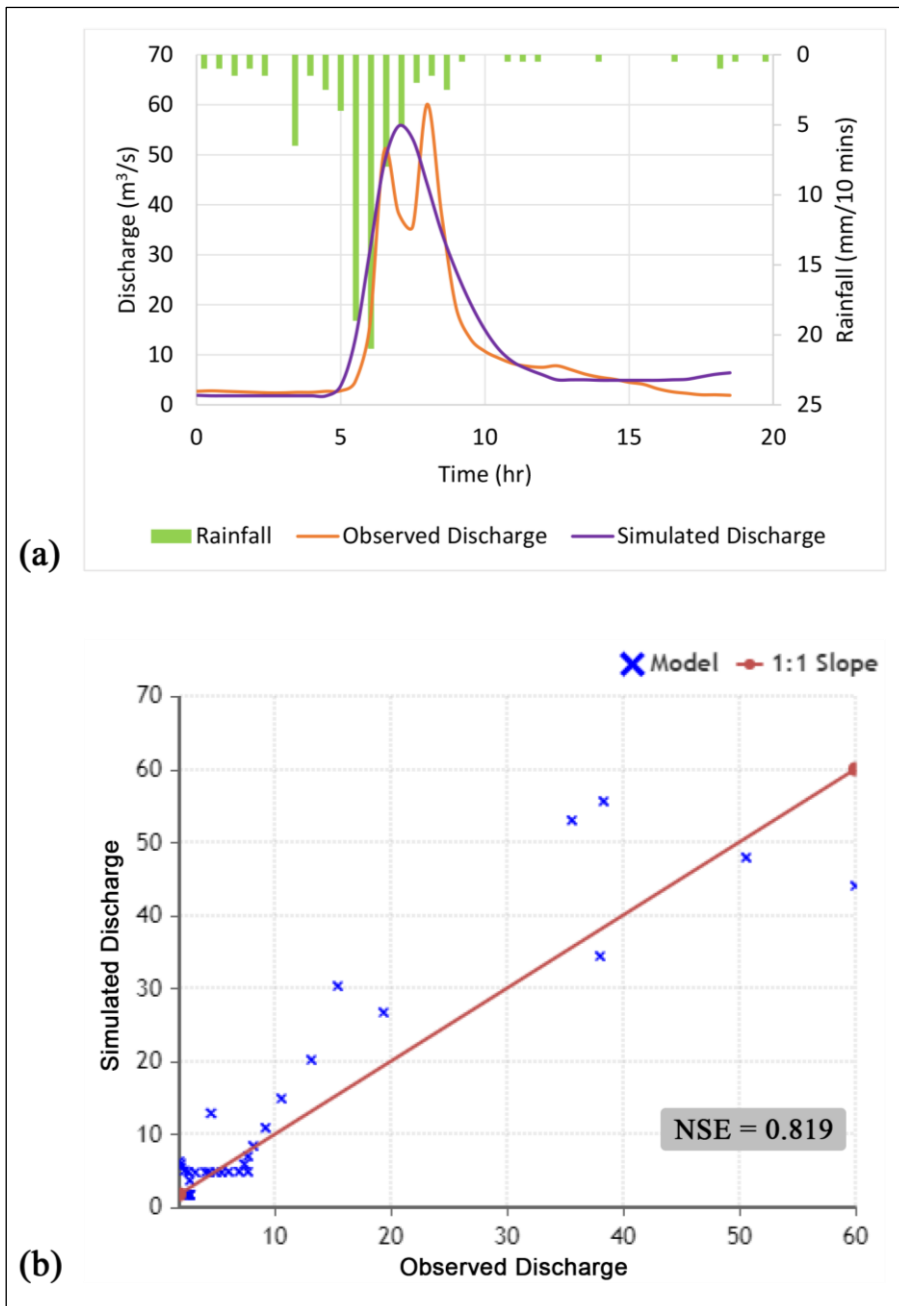
Figure 37. Validation of the calibrated parameters based on the 2021/01/26 rainfall event and its NSE coefficient.
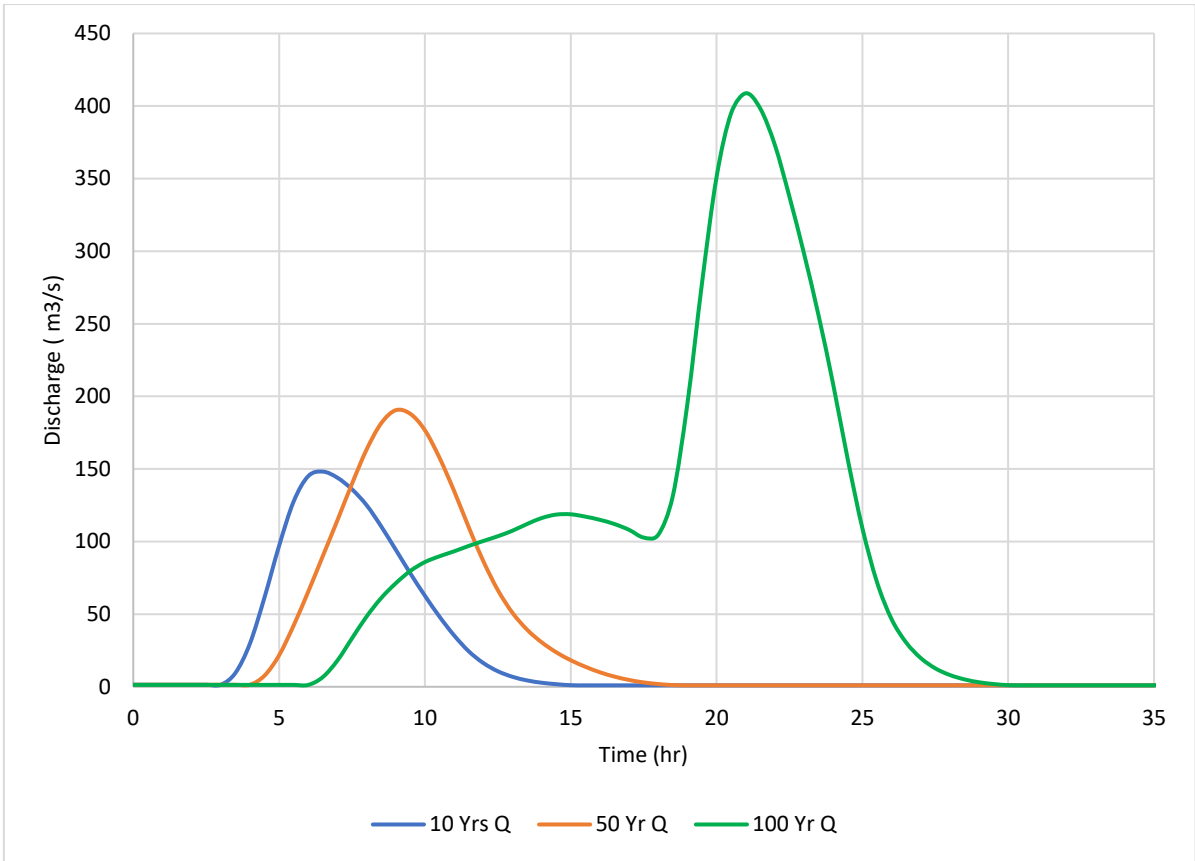
Figure 38.Generated discharge for the 10-, 50-, and the 100-year return period.

4.7 Stage and inundation analysis

Flood was simulated on both original and modified terrain with a return period of 10-, 50-, and 100-years. Figure 39 shows the topographic map of the original and modified terrain. It also shows where sand is being extracted. Discussed below are the results:

Flood simulated for the return periods shows an increase in the inundated area both on the original and modified terrain. Interesting phenomena were observed when simulations were done on the modified terrain. With the same amount of discharge for each return period, simulations were done on the modified −1, −2, and −3m terrain. Figure 40 to Figure 43 shows the results of the simulations. Figure 44 shows the location on the modified terrain where water level depth is being observed. Figure 45 shows that the water level increased by 2m for the 10-years return period, 4m for the 50-years return period, and 4.2m for the 100-years return period. On the −2 and −3m terrain depth, the 10-, 50-, and 100-year flood events share the same results with the −1m depth.

The first reason is that the upstream and downstream boundary elevation of the extraction sites are kept constant while only the area in between is deepened. By increasing the channel depth, the volume of water the site can contain also increases. If additional water is added, the outcome will be the same despite the extraction site depth.

The second reason is that the selected sand extraction sites along the channel already has a higher bank. Therefore, when deepening the channel and keeping the upstream and downstream elevation of the extraction site constant, the excess water is only kept within the higher river banks resulting in no change in the inundated area but the depth within the extraction site.

The results show that even though the terrain is being modified to accommodate sand extraction with different depths, flood results remain the same for the return periods.

Therefore, choosing an appropriate sand extraction site is a significant part of the mining process. Sand properties and stream velocity are factors that needed to also be considered. It is equally important to select a site that will have a minimal effect on flooding. As seen in the study results, channels with higher riverbanks and winder floodplain can be used as sand extraction sites as they could help reduce inundation.

Another phenomenon observed during the simulation is that when the channel is modified, changes in stream-stage occur further upstream of the river. The stage increases along with the return periods. At present, the assumption is that the model becomes unreliable when simulating a larger discharge amount over a narrow channel. The other possible reason could be the limited number of cross-sections used in this research. It could also be the result of the selected time step used in this study. However, further investigation is needed to verify if modifying the downstream of La Colle river affects stream-stage on the upstream of the river.
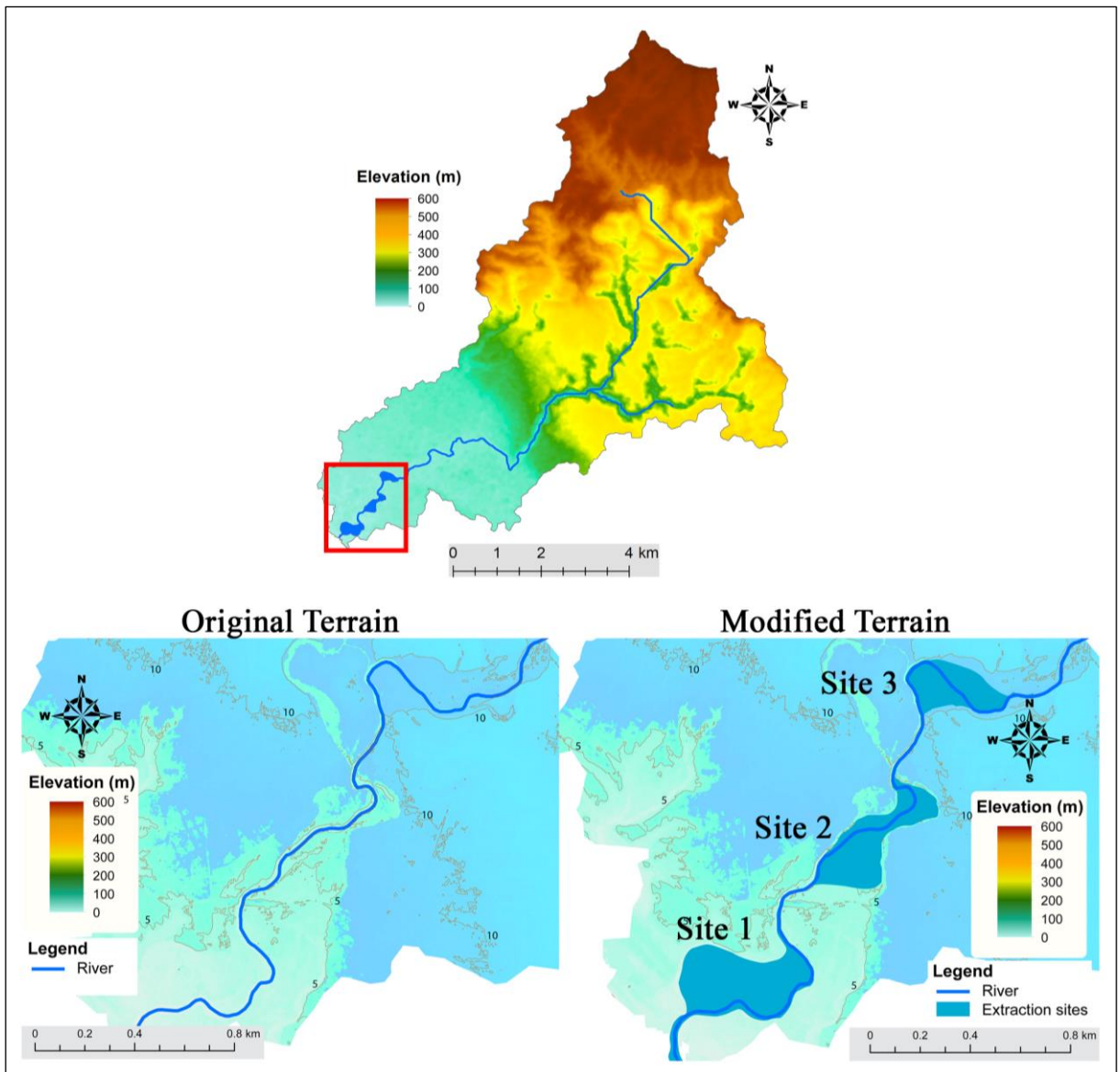
Figure 39. Map showing the difference between the original and modified terrain.
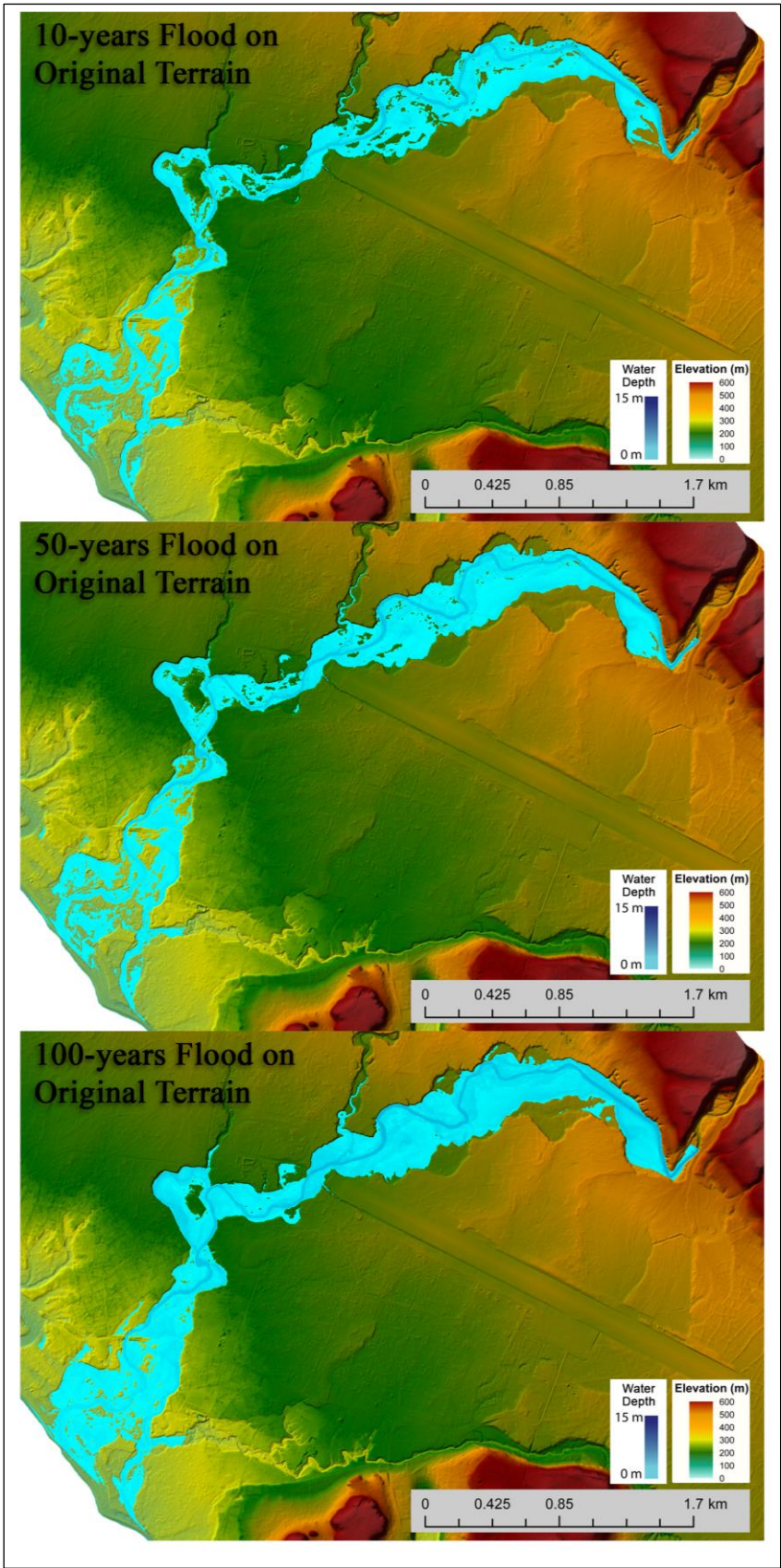
Figure 40. Flood simulation results for the 10-, 50-, and 100-year return period on the original terrain.
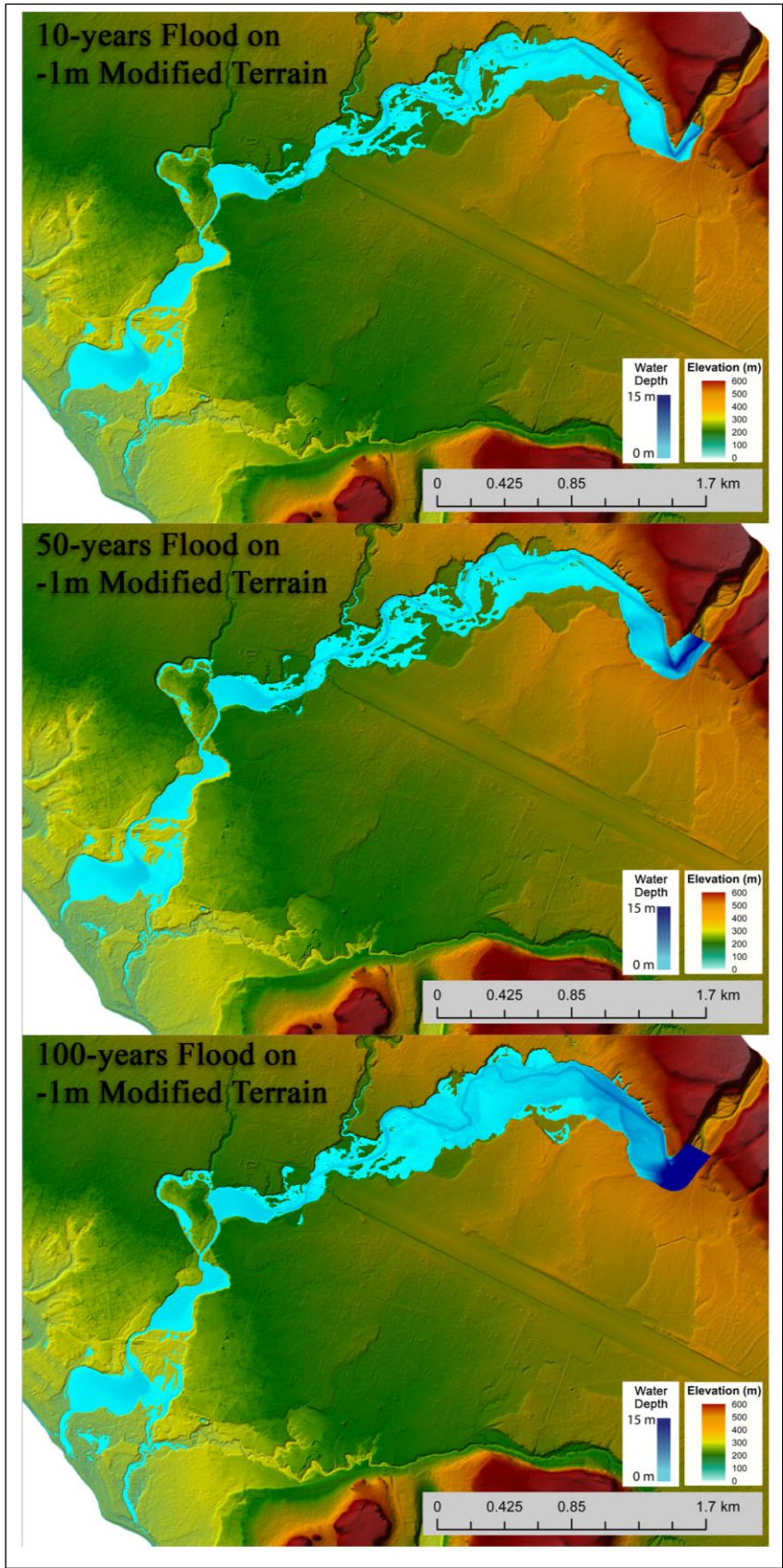
Figure 41. Flood simulation results for the 10-, 50-, and 100-year return period on the −1m modified terrain.
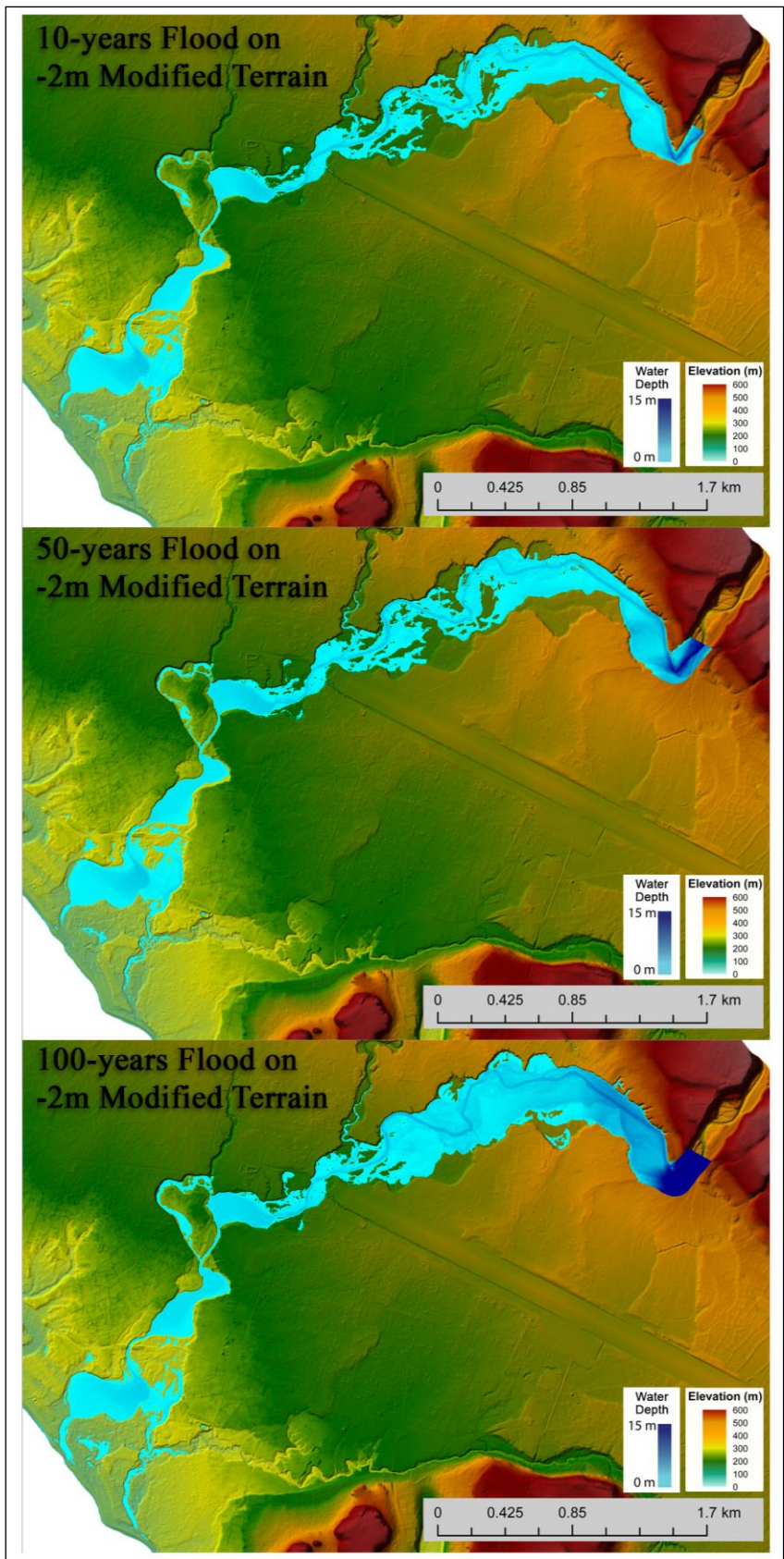
Figure 42. Flood simulation results for the 10-, 50-, and 100-year return period on the −2m modified terrain.
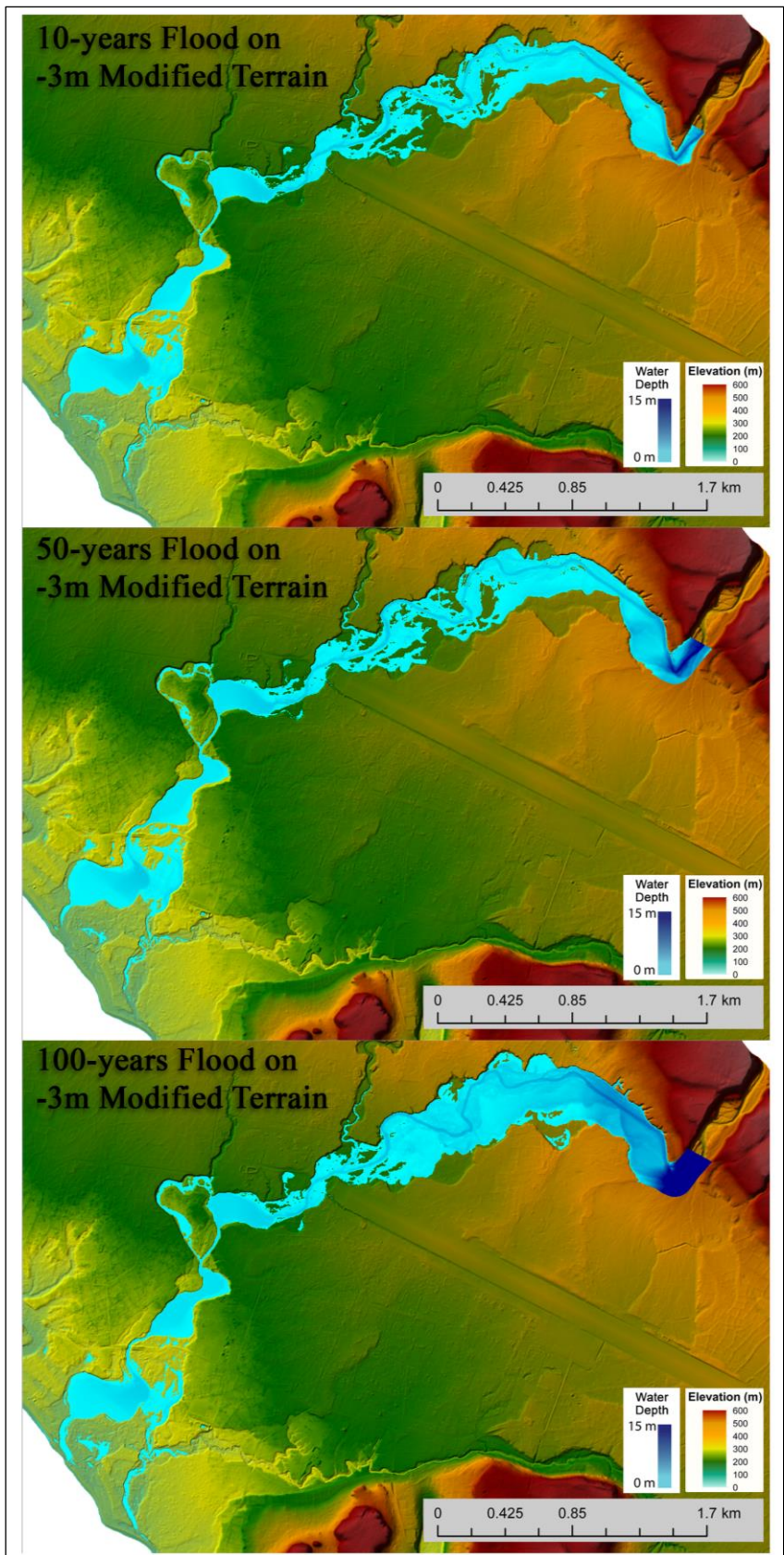
Figure 43. Flood simulation results for the 10-, 50-, and 100-year return period on the −3m modified terrain.
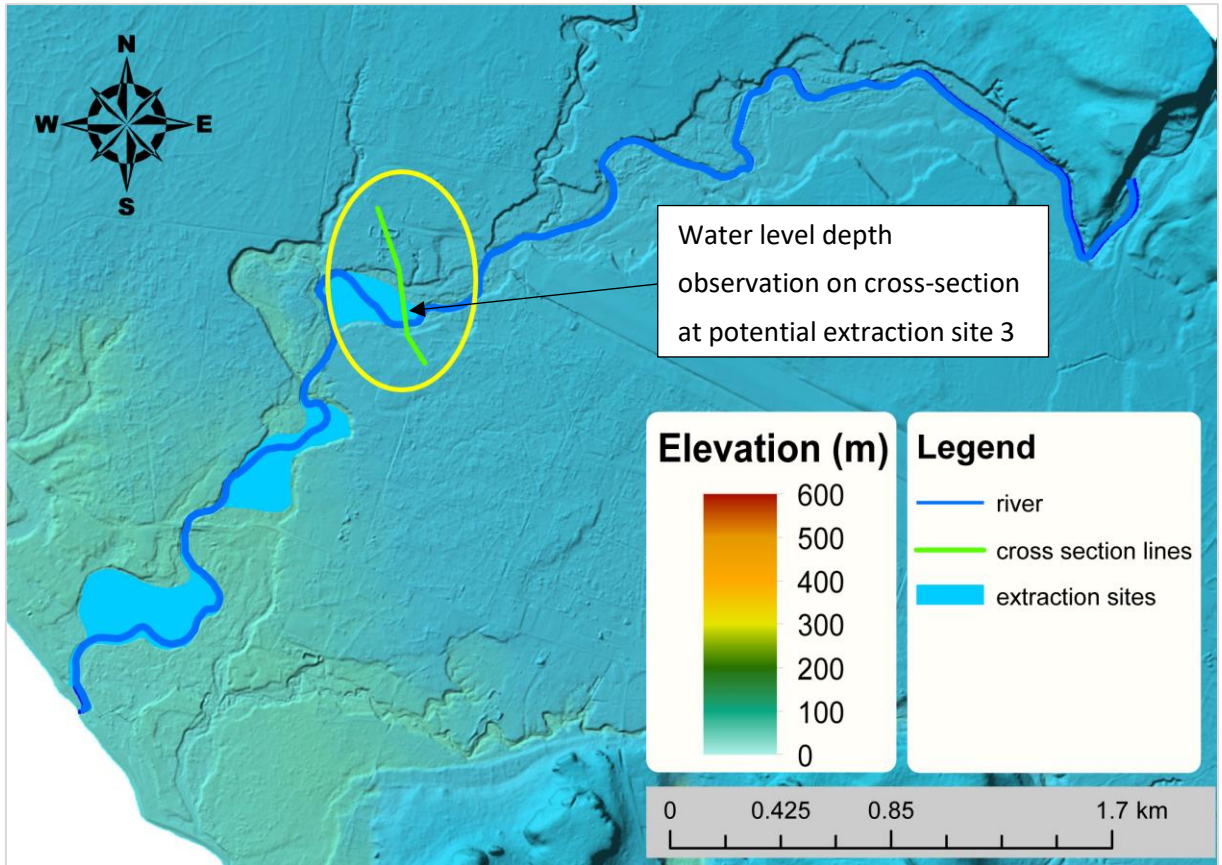
Figure 44. Location of channel cross-section where changes in flood water level are observed.
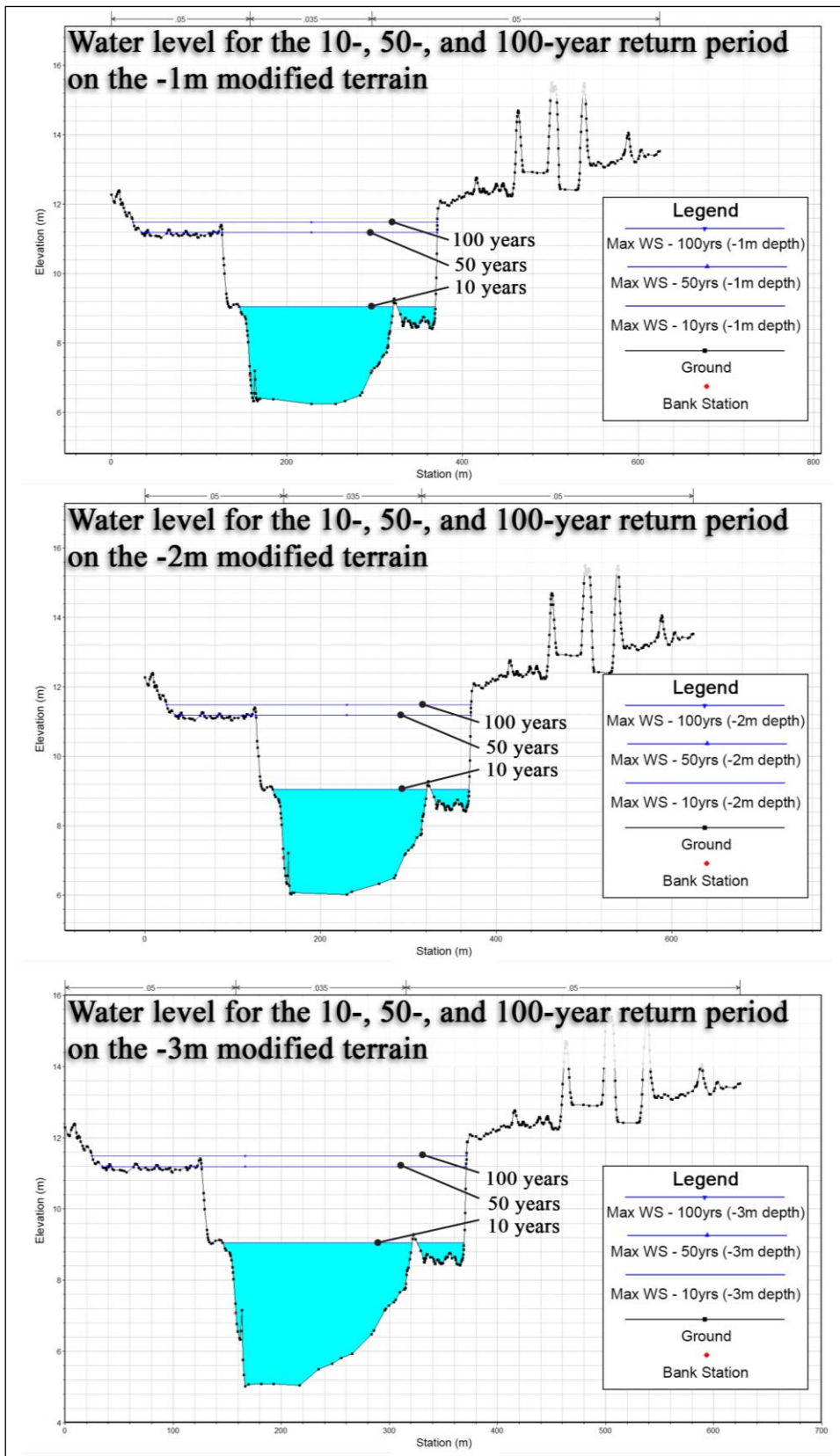
Figure 45. Change in water level for the flood return periods on the modified terrains.

4.8 Sand mining influence on flood analysis

Results show that for the 10-, 50-, and 100-year flood return period on the original terrain, inundated area increased from 0.8, 0.9, to 1.6 km^2, respectively. However, for the modified terrains, the area remained unchanged despite the change in extraction site depth. Total inundated areas for the modified terrain with −1, −2, and −3m were 1.01, 1.08, and 1.31km^2, respectively. This affirmed what previously discussed that deepening the extraction site to −3m will have the same impact on flood as the −1m depth.

Figure 46 also shows that from 10-, to the 66-year flood return period, the original terrain had a smaller inundated area while the modified terrains have a larger inundated area size. Past the 66-year return period, the modified terrains had a lesser inundated area compared to the original terrain. A possible reason why this happened is that since the channel is modified in areas with already a higher riverbank, they are more stable in handling excess discharge. In comparison, the original terrain allows excess water to flow over the lower riverbanks, thus freely expanding the inundated area.

Model simulation on floods with a return period of up to 30-years has been validated in this study. The result shows that the flood map in Figure 28 could only be trusted within this range.

Study results and analysis shows that sand extraction does and does not affect flooding along La Colle river. Current sand extraction activity along La Colle will not affect flooding as it is a controlled, small scale sand mining. Expanding mining activity to sites 2 and 3 could affect flooding. This study also shows that it is crucial to select sand extraction sites properly. If carefully chosen, the sites could reduce flood. Therefore, careful consideration must be made on potential sand mining sites before sand mining activities began.
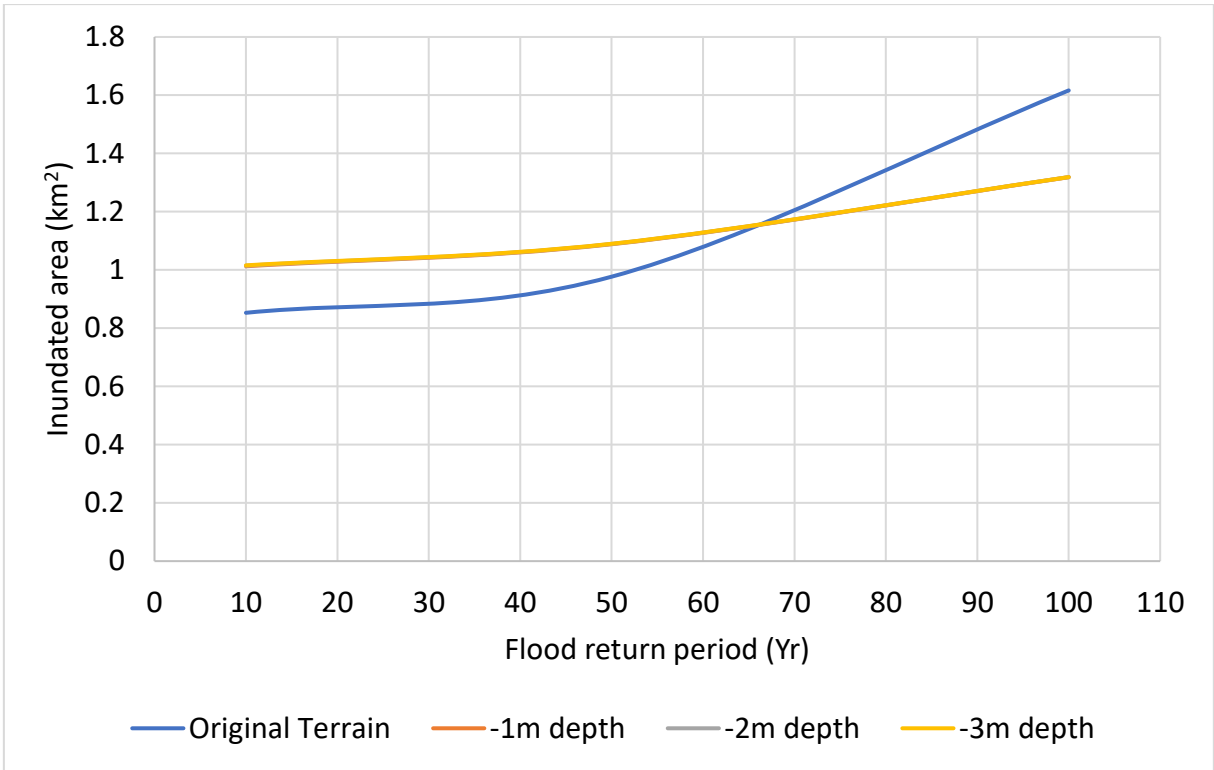
Figure 46. Inundated area size for flood return periods on the original and modified terrain.

CHAPTER FIVE: CONCLUSIONS

5.1 Introduction

The research investigates the relationship between sand mining and flooding on La Colle river. The major objective is to simulate flooding based on sand mining activities on the river. This chapter contains the research conclusions as well as the limitations and recommendations.

5.2 Conclusions

Sand mining's impact on flooding along La Colle river is the focus of this research. Field investigations, hydrological, and meteorological analyses were performed in order to determine the outcome of this study. The results revealed that sand mining could both influence and not influence flooding on La Colle river.

Sand mining could influence flooding in the following ways:

- By widening the extraction sites to the edge of the flood-prone zone, a flood with a 10-, 50-, or 100-year return period could be contained within the extraction site. Thus, reducing inundation extent in several places along the river.
- Deepening the channel at the sites to a depth of -1, -2, or $-3m$ while maintaining the channel elevation at the upstream and downstream boundaries of the site could also reduce flooding.

Sand mining would not influence flooding by:

- Setting an absolute minimum elevation for how deep an extraction can go. Since the results show no difference due to depth change, a $-1m$ depth and much smaller extraction sites would not influence flooding.
- Current sand mining practice on La Colle river will not affect flooding. This is because it is a controlled, small-scale sand mining activity.

So, regardless of the circumstances, flooding along La Colle river with regards to sand mining needs further investigations, more simulations, continuous monitoring, and closely regulated so that properly informed decisions can be made.

5.3 Recommendations and Limitations

- A proper hydrological database must be built where technical individuals from selected government departments could have access to.
- Flooding is an ongoing issue encountered during the cyclone seasons. Therefore, the government needs to urgently revive the appropriate Division responsible for hydrological data collection, whereby necessary analysis could be done to assist the relevant authorities.

- Correct and digitize all meteorological and hydrological data in the archives, as they will be needed shortly.
- The Vanuatu Government needs further investigations under the Ministry of Lands & Natural Resources and the Ministry of Climate Change. These investigations may not directly link to flooding or sand mining, but in the field of Hydrogeology and Hydrometeorology in order to combat future-related issues.

This research has several limitations. First, the insufficiency of past hydrological data. Analyzed events in this study excluded past extreme flood events as there were no hydrological data available.

Second, the scarcity of hydrogeological data. There were very little data available regarding groundwater movement within the watershed. Soil properties, characteristics, and infiltration rate are some of the much-needed data in this research. Estimating these factors in this research may also influence runoff modeling.

Third, not enough extreme events with both hydrological and meteorological data with regards to flooding. Reviewing past datasets indicated that rainfall was recorded on an hourly interval while river discharge was recorded on a 30-minute interval. However, in most past extreme events, either of the two datasets will not be available. Therefore, analysis of such an event becomes difficult, hence a limiting factor.

References

ADB. 2010. *Responding to Climate Change in the Pacific: Moving from Strategy to Action.* Mandaluyong: Asian Development Bank, 1-4. https://www.adb.org/sites/default/files/publication/28008/responding-climate-change.pdf.

Andrei, A, B Robert, and B Erika. 2017. "Numerical Limitations of 1D Hydraulic Models Using MIKE11 or HEC-RAS software – Case study of Baraolt River, Romania." *IOP Conference Series: Materials Science and Engineering* (IOP Publishing Ltd) 245 (7): 2-8.

Asabonga, M, B Cecilia, M C Mpundu, and N D Vincent. 2016. "The physical and environmental impacts of sand mining." *Transactions of the Royal Society of South Africa* 72 (1): 1-5. doi:https://doi.org/10.1080/0035919X.2016.1209701.

Azouagh, A, and I Hilal. 2018. "Integration of GIS and HEC-RAS in Floods Modeling of Martil River (Northern Morocco)." *European Scientific Journal* 14 (12): 130-142. doi:DOI: 10.19044/esj.2018.v14n12p130.

Barbalho, F D, F N Gabriela, and K Formiga. 2014. "Average Rainfall Estimation: Methods Performance Comparison in the Brazilian Semi-Arid." *Journal of Water Resource and Protection* 06 (2): 97-103.

Beca, GNS Science, and NIWA. 2015. *Draft Hazard and Risk Maps and Geo data Report: Risk Mapping and Planning for Urban Preparedness.* Hazard and Risk Maps, Auckland: BECA.

Beretta, Riccardo, Giovanni Ravazzani, Carlo Maiorano, and Marco Mancini. 2018. "Simulating the Influence of Buildings on Flood Inundation in Urban Areas." *Geosciences (Switzerland)* 8 (3): 77.

Betsholtz, A, and B Nordlof. 2017. *Potentials and limitations of 1D, 2D and coupled 1D-2D flood modelling in HEC-RAS.* Lund: Lund University.

Beven, K J. 2012. *Rainfall-Runoff Modelling: The Primer.* 2nd. Wiley-Blackwell.

Borsanyi, P. 2014. *ResearchGate: Questions.* February 4th. Accessed November 5th, 2020. https://www.researchgate.net/post/Does_taking_the_river_sand_when_the_water_level_in_the_river_reduced_have_a_positive_or_negative_impact.

Brock, C. 1998. *Towards Sustainable Forestry.* Canberra: Australian National University.

Brunner, G W. 2016. *HEC-RAS river analysis system: hydraulic reference manual.* California: US Army Corps of Engineers.

Chaudhry, M H. 2008. *Open-Channel Flow.* Columbia: Springer.

Damant, C, G L Austin, A Bellon, and R S Broughton. 1983. "Erros in the Thiessen technique for Estimating Areal Rain Amounts Using Weather Radar Data." *Journal of Hydology* 62 (1-4): 81-94. doi:http://dx.doi.org/10.1016/0022-1694(83)90095-1.

Dhakwa, C A, C A Biney, and K A. A D. G. Johnson. 2009. "Impact of mining operations on the ecology of river Offin, Ghana." *West African Journal of Applied Ecology* 7 (1): 19-30.

DID. 2009. *River Sand Mining Management Guideline.* Kuala Lumpur: Department of Irrigation and Drainage (DID), 18-44.

Dupre, W R. 2020. *Flooding, Erosion, and Sedimentation Issues Related to Sand and Gravel Mining.* Houston: University of Houston.

EIA. 2012. *Environmental Impact Assessment (EIA); Guidelines for River Sand and Stone Mining.* Sabah: Environment Protection Department.

Eidukat, B S. 1997. *Flood Frequency Analysis and Determination of 100-year and 500-year Floods.* April 9th. Accessed November 23rd, 2020. https://www.ndsu.edu/pubweb/~sainieid/group/100-year.htm.

Eko, K, A M Elfeki, and K Marko. 2016. "Spatial Modelling of Flood Inundation, Case Study of Pesanggrahan Floodplain, Jakarta, Indonesia." *Journal of Geography, Environment and Earth Science International* 5 (3): 1-10.

Enea, A, A Urzica, and I G Breaban. 2018. "Remote Sensing, GIS and HEC-RAS Techniques, Applied for Flood Extend Validation, based on LANDSAT Imagery, LiDAR and Hydrological data. Case Study: Baseu river, Romania." *Journal of Environmental Protection and Ecology* 19 (3): 1091–1101.

Feldman, A D. 2000. *Hydrological Modeling System HEC-HMS.* Washington: US Army Corps of Engineers.

GSI. 2014. *A Model document on Impacts and Methodology of Systematic and Scientific Mining of the River bed material.* Geological Survey of India, 1-5.

Henderson, F M. 1996. *Open Channel Flow.* New York: MacMillan Publishing Co. Inc.

Kokkenen, T, H Koivusalo, and T Karvonen. 2001. "A semi-distributed approach to rainfall-runoff modelling - a case study in a snow affected catchment." *Environmental Modelling & Software* 16 (5): 481-493. doi:http://dx.doi.org/10.1016/S1364-8152(01)00028-7.

Kondolf, G M. 1994. "Environmental planning in regulation and management of instream gravel mining in California." *Landscape and Urban Planning* 29 (2-3): 185-199.

Kori, E, and H Mathada. 2012. "An Assessment of Environmental Impacts of Sand and Gravel Mining In Nzhelele Valley, Limpopo Province, South Africa." *2012 3rd*

International Conference on Biology, Environment and Chemistry. Singapore: IACSIT Press. 1-5.

Langer, W H. 2003. *A General Overview of the Technology of In-Stream Mining of Sand and Gravel Resources, Associated Potential Environmental Impacts, and Methods to Control Potential Impacts.* U.S. Geological Survey Open-File Report 02-153, U.S. Department of the Interior | U.S. Geological Survey.

Lundgren, L. 1986. *Environmental Geology.* New Jersey: Englewood Cliffs.

Mai, N, P James , and M A Myo. 2019. "From Tibet to the 'Nine Dragons', Vietnam's Mekong Delta is losing sand." *Sand Mining is Destroying Asia's Rivers* 15-122.

Mccool, J, and A Woodward. 2015. "Eye health outreach services in the Pacific Islands region: An updated profile." *The New Zealand Medical Journal* 128 (1420): 25-33. https://www.researchgate.net/publication/281778505_Eye_health_outreach_services_in_the_Pacific_Islands_region_An_updated_profile/figures?lo=1.

Mimura, N. 1999. "Vulnerability of island countries in the South Pacific to sea level rise and climate change." *Climate Research* 12: 137-143. https://www.int-res.com/articles/cr/12/c012p137.pdf.

Mngeni, A, C Betek, C Musampa, and M Nakin. 2016. "The physical and environmental impacts of sand mining." *Transactions of the Royal Society of South Africa* 72 (1): 1-5.

Nash, J. 1958. "Determinig Run-off From Rainfall." *Proceedings of the Institution of Civil Engineers* 10 (2): 163-184.

Nurhasan, U, and P Y Saputra. 2018. "Analysis of Sand Mining Areas in Lumajang Using WEBGIS." *Proceedings of the 2018 International Conference on Energy and Mining Law (ICEML 2018).* Amsterdam: ATLANTIS PRESS. 2352-5428.

NZG. 2010. *Tools for Estimating the Effects of Climate Change on Flood Flow.* New Zealand Government, 35-39.

OCS. 2005. *Determining Return Periods.* Oklahoma: Oklahoma Climatological Survey, 1-2.

Osanloo, M, and M Minaei Mobtaka. 2014. "Positive impacts of mining activities on environment." *Beijing International Symposium on Land Reclamation and Ecological Restoration (LRER 2014).* Beijing. 1-8.

Rehak, B. 2019. *Reduce Flood Now.* April 4th. Accessed January 22nd, 2021. https://reduceflooding.com/2019/04/15/caution-sb-2126-opens-door-to-sand-mining-in-rivers/#:~:text=SB%202126%20would%20allow%20a,long%20as%20it's%20on%20private.

Rinaldi, M, B Wyzga, and N Surian. 2005. "Sediment mining in alluvial channels: physical effects and management perspectives." *River Research and Applications* 21 (7): 805-828. doi:https://doi.org/10.1002/rra.884.

SANDRP. 2019. *Sand Mining issues Proliferate even in Monsoon.* September 9th. Accessed December 24th, 2020. https://sandrp.in/2019/09/09/drp-nb-8-sept-2019-sand-mining-issues-proliferate-even-in-monsoon/.

Saviour, M N, and P Stalin. 2012. "Soil and Sand Mining: Causes, Consequences and Management." *IOSR Journal of Pharmacy (IOSRPHR)* 2 (4): 1-6.

Sitterson, J, C Knightes, R Parmar, K Wolfe, M Muche, and B Avant. 2017. *An Overview of Rainfall-Runoff Model Types.* Athens: United States Environmental Protection Agency, 13-15.

SPREP. 2001. "Vanuatu." *SPREP.*
https://www.sprep.org/att/IRC/eCOPIES/Countries/Vanuatu/68.pdf.

Stebbins, M. 2006. *Can gravel mining and water supply wells coexist.* University News, Maine: University of Maine News Reports.

TACA. 2018. *Societal and Environmental Benefits of Sand and Gravel Mining.* White Paper, Texas: Texas Aggregate and Concrete Association. https://reduceflooding.com/wp-content/uploads/2018/06/TACA-White-Paper.pdf.

Thiessen, A H. 1911. "Precipitation for Large Areas." *Monthly Weather Review* 39: 1082-1084.

UNEP. 1991. *Environmental aspects of selected non-ferrous metals (Cu, Ni, Pb, As) ore mining. A technical guide.* UNEP Technical report series No. 5, Paris: UNEP IE/PAC, 116.

UNU. 2015. "United Nations University, Institute for Environment and Human Security ." *World Risk Report 2015.*

USACE. 2000. *HEC-HMS User's Manual.* User's Manual, Davis: U.S. Army Corps of Engineers.

USDA. 1986. *Urban Hydrology for Small Watersheds.* Washington: U.S. Department of Agriculture.

VANSO. 2020. *Vanuatu National Statistics Office.* Accessed December 28th, 2020. https://worldpopulationreview.com/countries/vanuatu-population.

Vaze, J, P Jordan, R Beecham, A Frost, and G Summerell. 2012. "Guidelines for Rainfall-Runoff Modelling:Towards best practice model application." 47.

Vlok, W. 2016. *ResearchGate: Questions.* June 10th. Accessed November 4th, 2020. https://www.researchgate.net/post/Does_taking_the_river_sand_when_the_water_level_in_the_river_reduced_have_a_positive_or_negative_impact.

Willison, J.H Martin. 2014. *ResearchGate: Questions.* February 5th. Accessed November 4th, 2020.
https://www.researchgate.net/post/Does_taking_the_river_sand_when_the_water_leve l_in_the_river_reduced_have_a_positive_or_negative_impact.

Work, P A. 2016. "Sand Mining/Beach Sand Mining. In: Kennish M.J." *(eds) Encyclopedia of Estuaries. Encyclopedia of Earth Sciences Series* (Springer).
doi:https://doi.org/10.1007/978-94-017-8801-4_251.

WWF. 2018. *Uncovering Sand Mining's Impact on the world's rivers.* Enviromental Report, Gland: PHYS.ORG, 1-4. Accessed 11 27, 2020. https://phys.org/news/2018-08-uncovering-sand-impacts-world-rivers.html.

Yehalegaonkar, S K, M K Jose, and V Basappa. 2014. "A Study of Effect of Sand Mining on Riverine Environment." *Hydraulics, Water Resources, Coastal and Environmental Engineering.* Belgaum. 1378-1386.
https://www.researchgate.net/publication/297846336.

APPENDICES

APPENDIX A: HYDROLOGICAL DATA MINING REPORT

Hydrological Data Mining

By: Iuma Bani

University of Tsukuba

In finalizing my research, I received a set of hydrological data from the Department of Water Resources (DOWR) in Port Vila, Vanuatu. When reviewing the data and comparing it against my collected data, the results do not match. My field investigations data indicated that La Colle river's upstream stream depth is always less than a meter on a sunny day, but what was recorded in the hydrological data was consistently above 4 meters (fig. 1). However, when comparing the discharge measurements, they are somewhat similar, within the $1m^3$/s range.

Recorded water depth at upstream river gauge site

N°	Date	Hauteur Hm	Débit Q m³/s
93	22.08.1983	4,40	1,43
94	25.08.1983	4,44 – 4,46	1,86
95	25.08.1983	4,495	2,25
96	30.08.1983	4,39	1,32
97	06.09.1983	4,40	1,47
98	12.09.1983	4,39	1,35
99	19.09.1983	4,39	1,38
100	28.09.1983	4,38	1,36
101	06.10.1983	4,38	1,28
102	10.10.1983	4,38	1,18
103	17.10.1983	4,38	1,18
104	26.10.1983	4,40	1,31
105	03.11.1983	4,39	1,25
106	10.11.1983	4,39	1,26
107	17.11.1983	4,385	1,24
108	24.11.1983	4,39	1,26
109	02.12.1983	4,39	1,23

Fig. 1 – Extract from the ORSTOM report obtained from the DOWR.

To confirm that recorded depth, I went to the DOWR seeking answers. DOWR staff then directed me to a retired department staff, Mr. Stephen Morrison. Mr. Morrison has been working with the DOWR for over 30 years, building gravity water-fed systems all around Vanuatu. I tracked him down to his house and requested if he could clarify why the stream depth of 4+ meters with only an average discharge of just above $1m^3$/s.

Upon talking with Mr. Morrison, here are the things mentioned with regards to the stream depth.

When installing the sensor in the 1970s, La Colle river was the last to be installed. The instrument has different segments where it uses those different segments to measure the water level at each meter depth. Meaning, specific sections were used to measure water depth at different levels. Unfortunately, at that time, they were out of segments that were used to measure the depth from 0 to 4 m. They only had elements that would measure the depth from above 4m. therefore, the stream's actual depth would be 0.40m if it was recorded as 4.40m.

N°	Dates	Hauteur Hm	Corrected Stream depth (m)	Debit Q m³/s
93	22.08.1983	4,40	0.40	1,43
94	25.08.1983	4,44 – 4,46	0.44 – 0.46	1,86
95	25.08.1983	4,495	0.495	2,25
96	30.08.1983	4,39	0.39	1,32
97	06.09.1983	4,40	0.40	1,47
98	12.09.1983	4,39	0.39	1,35
99	19.09.1983	4,39	0.39	1,38
100	28.09.1983	4,38	0.38	1,36
101	06.10.1983	4,38	0.38	1,28
102	10.10.1983	4,38	0.38	1,18
103	17.10.1983	4,38	0.38	1,18
104	26.10.1983	4,40	0.40	1,31
105	03.11.1983	4,39	0.39	1,25
106	10.11.1983	4,39	0.39	1,26
107	17.11.1983	4,385	0.385	1,24
108	24.11.1983	4,39	0.39	1,26
109	02.12.1983	4,39	0.39	1,23

Fig. 2 – Table showing a sample of what the correct stream depth would be like after it is being corrected.

Since the ORSTORM report had a very good set of data that could be useful in future studies, I would highly recommend that the DOWR properly and correctly update the data accordingly to resist and minimize confusion in years to come.